

The Serpens Molecular Cloud

C. Eiroa

Dpto. Física Teórica, Universidad Autónoma de Madrid, 28049 Madrid, Spain

A. A. Djupvik

Nordic Optical Telescope, Apdo 474, 38700 Santa Cruz de La Palma, Spain

M. M. Casali

European Southern Observatory, Karl-Schwarzschild-Strasse 2, 85748 Garching, Germany

Abstract. The Serpens cloud has received considerable attention in the last years, in particular the small region known as the Serpens cloud core where a plethora of star formation related phenomena are found. This review summarizes our current observational knowledge of the cloud, with emphasis on the core. Recent results are converging to a distance for the cloud of $\sim 230 \pm 20$ pc, an issue which has been controversial over the years. We present the gas and dust properties of the cloud core and describe its structure and appearance at different wavelengths. The core contains a dense, very young, low mass stellar cluster with more than 300 objects in all evolutionary phases, from collapsing gaseous condensations to pre-main sequence stars. We describe the behaviour and spatial distribution of the different stellar populations (mm cores, Classes 0, I and II sources). The spatial concentration and the fraction number of Class 0/Class I/Class II sources is considerably larger in the Serpens core than in any other low mass star formation region, e.g. Taurus, Ophiuchus or Chamaeleon, as also stated in different works. Appropriate references for coordinates and fluxes of all Serpens objects are given. However, we provide for the first time a unified list of all near-IR sources which have up to now been identified as members of the Serpens core cluster; this list includes some members identified in this review. A cross-reference table of the near-IR objects with optical, mid-IR, submillimeter, radio continuum and X-ray sources is also provided. A simple analysis has allowed us to identify a sample of ~ 60 brown dwarf candidates among the 252 near-IR objects; some of them show near-IR excesses and, therefore, they constitute an attractive sample to study very young substellar objects. The review also refers to the outflows associated with the young sources. A section is dedicated to the relatively small amount of works carried out towards Serpens regions outside the core. In particular, we refer to ISO and to recent Spitzer data. These results reveal new centers of active star formation in the Serpens cloud and the presence of new young clusters, which deserve follow-up observations and studies to determine their characteristics and nature in detail. Finally, we give a short, non-exhaustive list of individually interesting Serpens objects.

1. Introduction

A considerable amount of work has been dedicated to the region known as the Serpens dark cloud (Galactic coordinates $l^{II} = 32^\circ$, $b^{II} = 5^\circ$) since it was recognized by Strom

et al. (1974) as a site of active star formation. The cloud extends several degrees around the young variable star VV Ser and forms part of the large local dark cloud complex called the Aquila Rift, which has been extensively mapped in several molecular line surveys (e.g. Dame & Thaddeus 1985, Dame et al. 1987, 2001, see the chapter by Prato et al.). A large scale extinction map has been presented by Cambr esy (1999) and Dobashi et al. (2005). Serpens is seen on optical images as a large area irregularly obscured by large amounts of dust; Fig. 1 reproduces the DSS R band photograph of a region $2^\circ \times 2^\circ$ in size. Several reflection nebulosities are distinguished, the most prominent of which are S 68 (Sharpless 1959, see also Dorschner & G urtler 1963, van den Bergh 1966, Bernes 1977), illuminated by HD 170634, and a very red bipolar, reflection nebulosity, usually referred to as the Serpens object, the Serpens nebula, or the Serpens reflection nebulosity (SRN), illuminated by the pre-main sequence star SVS 2 (Strom et al. 1974, 1976, Worden & Grasdalen 1974, King et al. 1983, Warren-Smith et al. 1987, G omez de Castro et al. 1988). In this work, we will refer to that nebulosity as SRN.

Relatively little work has been devoted to studying the large scale properties of the Serpens cloud, having been mainly concentrated around SRN and VV Ser, which are located towards the North of the large extinction map analysed by Cambr esy (1999). Cohen & Kuhl (1979) and Chavarr ıa et al. (1988) conducted optical studies of the region and identified several $H\alpha$ emission line stars and some B, A and later spectral type stars associated with reflection nebulae. Loren et al. (1979) carried out a 2.6 mm line CO map over an area of ~ 300 square arc minutes and detected a dense H_2CO core of $\sim 3'.3$ in radius centred in SRN. IRAS maps of a $\sim 3^\circ \times 3^\circ$ region around the cloud core show large scale extended far-IR emission and several point-like sources associated with some visible and invisible stars (Zhang et al. 1988b). The cloud core with several point-like sources embedded in extended emission shows up very prominently in all IRAS bands (Zhang et al. 1988a). More recently Schnee et al. (2005) have analysed recalibrated IRAS data to estimate dust column densities and dust temperatures. Assuming a distance of 700 pc to Serpens, Zhang et al. (1988b) estimate a total far-IR luminosity from the whole Serpens cloud of $\sim 3200 L_\odot$ and the dust mass inferred from the extended emission is $\sim 290 M_\odot$. The actual distance to Serpens is most likely significantly smaller than the value assumed by Zhang et al. and, therefore, the luminosity and dust emitting mass should be corrected. In fact, the distance to Serpens has been a controversial point over the years, with suggested figures in the range from ~ 200 pc to ~ 700 pc. At present, a smaller distance value is commonly accepted. We analyse this issue in the next section.

After the discovery of the cloud core, observational efforts have concentrated in that area. The reason is the extreme richness in star formation activity found in the core, with all relevant phenomena taking place in a small region of just few arc minutes in diameter: pre-protostellar gaseous condensations; pre-stellar dust condensations; Class 0, Class I and Class II objects; different evidences of infalling gas; disks; molecular and atomic outflows and jets; clustering of young stellar objects (YSOs) in different evolutionary stages, etc. The Serpens core indeed represents a unique laboratory for studies of star formation processes and observable phenomena, and the inter-relation between them.

A first review article of the most relevant observational results up to ~ 1991 was written by us (Eiroa 1991). In this new contribution we concentrate mainly on results achieved during the last 15 years. We review observations related to the Serpens core

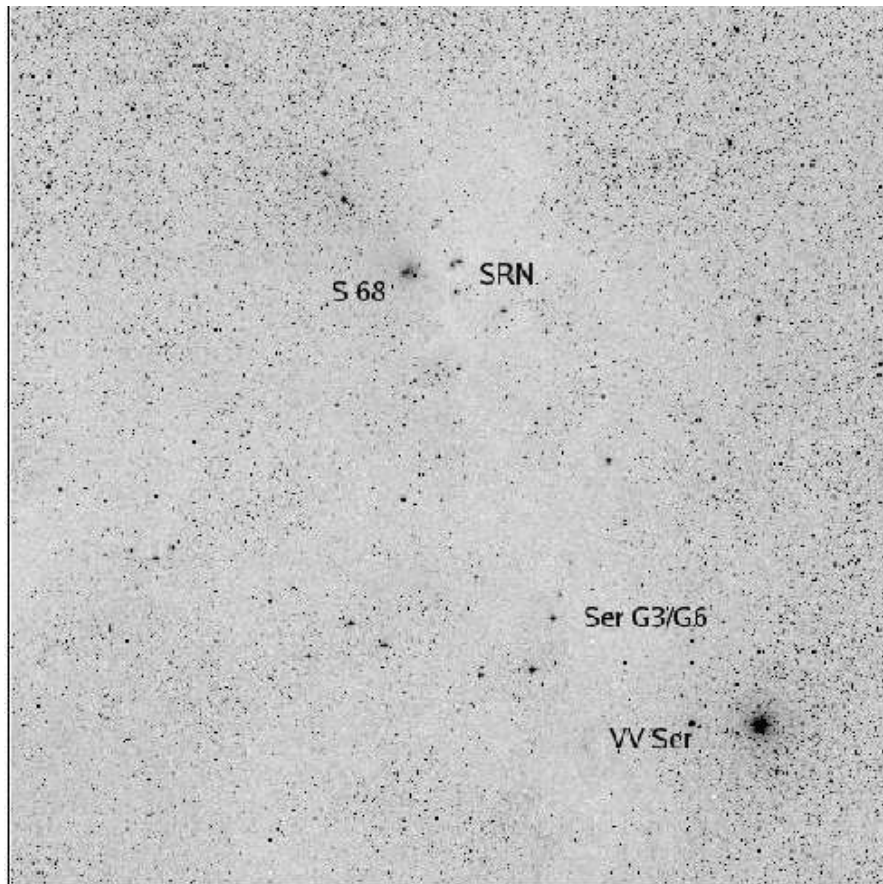


Figure 1. The Serpens molecular cloud as seen on the DSS *R*-band plates. Large scale irregular dark structures are clearly seen. The reflection nebulosities S 68 and SRN are indicated, as well as the position of VV Ser and of the $H\alpha$ emission line stars Ser G3/G6. Field size is $2^\circ \times 2^\circ$. Field centre: $\alpha_{2000} = 18^h 30^m$, $\delta_{2000} = 0^\circ 50'$. North to the top, East to the left. The image has been downloaded from the Canadian Astronomy Data Center (<http://cadwww.dao.nrc.ca/dss>).

in particular, since this part of the cloud has continued to be the focus of the large observational effort carried out by many different research groups. Nonetheless, a section is also dedicated to recent work carried out in Serpens areas outside the core. The new results confirm and emphasize the role of Serpens as a key region for detailed studies of star formation and the understanding of all related phenomena.

2. The Distance of Serpens

The distance to Serpens has been a matter of controversy over the years. Until 1996 the distance to the Serpens molecular cloud was estimated from a handful of stars associated with reflection nebulae. Mainly through disagreements on spectral type and luminosity classes, the different distances obtained were the subject of much debate

(see Straizys et al. 1996 for details). Racine (1968) gave a first distance estimate (440 pc) based on the star HD170634 which he classified as a B7 V star. Strom et al. (1974) found the same distance to the same star independently from their IR data classifying it as an A0 (V.). Chavarría-K et al. (1988) obtained spectroscopy, $uvby\beta$ and JHKLM photometry for this one (A1 V) and three more stars: SAO 123590 (B4 V), SAO 123595 (B3 V), and SAO 123661 (B3), and obtained a distance of 245 ± 30 pc. Zhang et al. (1988), however, estimated 700 pc (with a large scatter) for three of the above four stars, having assigned luminosity class III (citing an unpublished reference) and found support from kinematics (CO and NH₃ lines). De Lara & Chavarría (1989) rechecked their spectra and confirmed the main sequence nature of the above sources, and moreover estimated $d = 296 \pm 34$ pc based on 7 stars. Excluding HD170634 (claiming it to be a shell star) and adding two other reflection nebulae stars [CDF88] 1 and [CDF88] 7 de Lara et al. (1991) arrived at $d = 311 \pm 38$ pc and a mean total to selective extinction ratio $R = A_V/E(B - V) = 3.3 \pm 0.3$. This estimate was in use until Straizys et al. (1996) revised the distance using a completely independent method. They surveyed photometrically most stars down to magnitude 13 in a 6.5 square degrees region in the Vilnius photometric system of seven narrow bands (*UPXYZVS*). Spectral types and absolute magnitudes were found for 105 stars - of which 18 belong to the cloud. This sample included the earlier used stars, and it was noted that both SAO 123590 and SAO 123661 are close binaries. Applying the total to selective extinction ratio found by de Lara et al. (1991) for the stars in or behind the molecular cloud they found a distance of 259 ± 37 pc. This estimate was also supported by Festin (1998) who made use of the cloud as a screen when searching for foreground dwarfs in a 0.15 square degree area about 4 degrees to the South of the Cloud Core. Straizys et al. (2003) then investigated 473 stars across a larger area (5×10 degrees) and found the front edge of the clouds in this area to be at 225 ± 55 pc and the cloud complex possibly 80 pc deep. These are believed to be part of the Aquila Rift large dark cloud complex, located at a distance of 200 ± 100 pc (Dame & Thaddeus 1985). Using 2MASS data Knude (2005) recently has estimated extinction and distances for 754 stars in the same area as that used by Straizys et al. (1996) and find a distance to the Serpens cloud of 210 ± 12 pc, estimating the extinction jump by using several physical indicators, among these the A_V vs. σ_{A_V} variation seen in MHD simulations. Thus, all recent and, likely, more reliable results are converging to a distance $\sim 230 \pm 20$ pc for the Serpens cloud.

3. An Overall Description of the Serpens Core

The early observations of Loren et al. (1979) found a nearly circular, high density H₂CO core approximately centred in SRN, while maps of the far-IR emission, NH₃ and other molecules showed a more elongated structure extending in a North-West/South-East direction with two broad peaks: a Southeastern (SE) clump with a broad peak close to SRN, extending towards the South from this object, and a second Northwestern (NW) clump peaking at a position close to the source FIRS 1, the most prominent object embedded in the Serpens core (e.g. Ho & Barrett 1980, Little et al. 1980, Nordh et al. 1982, Ungerechts & Güsten 1984, Harvey et al. 1984, Takano 1986, Zhang et al. 1988a, Torrelles et al. 1989). Estimated 60/100 μ m colour temperatures in the range $\sim 20 - 30$ K are similar to the kinematic gas temperatures found by Loren et al. (1979). The division of the internal structure of the gas and dust into two main subclouds or clumps has been confirmed by recent studies, including HIRES-IRAS images (Hurt & Barsony,

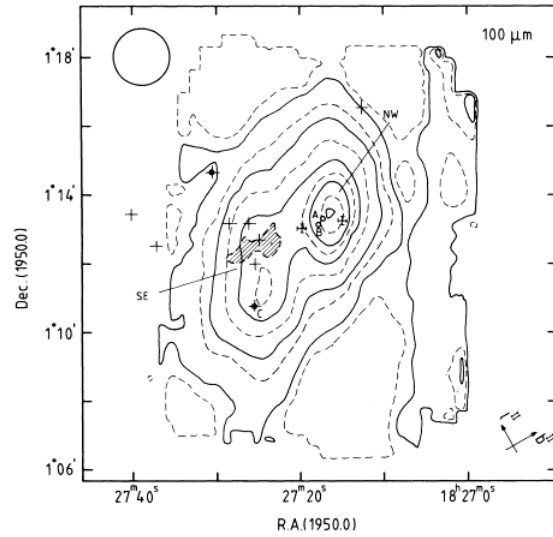


Figure 2. IRAS-CPC 100 μm map of the Serpens core (taken from Zhang et al., 1988a). The dashed region approximately represents the position of SRN.

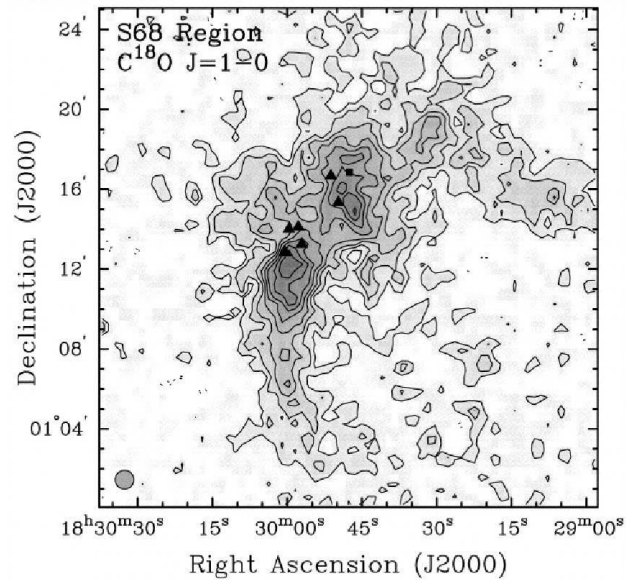


Figure 3. Integrated C^{18}O J=1-0 emission from the Serpens core (taken from McMullin et al., 2000). Black symbols represent some young embedded objects.

1996), submm/mm continuum maps (e.g. Casali et al. 1993, Davis et al. 1999, Kaas et al. 2004), and maps of several molecular lines coming from different isotopical species and tracing gas with different column densities, like CO, ^{13}CO , C^{18}O , H_2CO , HCO^+ , N_2H^+ , CS, HCN, etc. (e.g. McMullin et al. 1994, 2000, White et al. 1995, Testi et al., 2000). Fig. 2 and 3 show the IRAS and C^{18}O maps of the Serpens core respectively (Zhang et al. 1988a, and McMullin et al. 2000), where the extended core emission and the two broad SE and NW clumps of dust and gas show up very clearly. Davis et al. (1999) find some cavity-like submm structures (see Fig. 10); in particular, the most remarkable one is found between the NW and SE clumps (see also Fig. 11 in Kaas et al., 2004). In addition, small-scale gas and dust structures within each individual clump are seen in high resolution maps (e.g. Fig. 3). The complexity of the cloud core reflects density and temperature enhancements and the effects of the embedded stellar/protostellar population; Davis et al. (1999) suggest that the cavity-like submm structures may have been shaped by outflows from young objects in the core. Both NW and SE core clumps behave kinematically different (Testi et al. 2000); in this respect, it is interesting to note that the characteristics of the embedded YSO population within each individual clump show some differences, at least when the evolution of the sources is considered (see Sect. 5).

While there is an overall agreement between the results found by different groups concerning the structure, temperature, density and gas kinematics, a detailed comparison shows some points of disagreement. Those could be due to differences in beam sizes and/or the parameters and methods used to analyze the data. It would be interesting to clarify these discrepancies by carrying out new specific observations and analysis. Many molecules show self-absorbed line profiles in different core positions (see Loren & Wootten 1980 and Loren et al. 1981, for the earliest works), in particular close to embedded protostellar objects, and their kinematical behaviour suggests infall motions; furthermore, the SE and NW clumps seem to be undergoing global, large-scale (~ 0.2 pc) infalling motions (Williams & Myers 2000, Olmi & Testi 2002). The latter authors point out that the data are in qualitative agreement with the theoretical expectation of a slow contraction followed by rapid star formation in localized high density regions. A velocity gradient from East to West of $\sim 1 - 2 \text{ km s}^{-1} \text{ pc}^{-1}$ is observed in the most recent C^{18}O maps (McMullin et al. 2000, Olmi & Testi 2002), supporting the early NH_3 velocity gradient claimed by Ungerechts & Güsten (1984); in apparent contradiction with previous C^{18}O results (White et al. 1995), which did not find any evidence for such velocity gradient. Depending on the molecules and transition lines, temperatures are found in the range from ~ 15 K in the more diffuse parts of the core, up to ~ 50 K in condensations close to embedded young objects. The mean average temperature across the core is $\sim 25 - 30$ K (McMullin et al. 2000). These gas temperatures are similar to dust temperatures found across the cloud core and in the dust surrounding the embedded YSOs (e.g. Zhang et al. 1988a, Casali et al. 1993, Hurt & Barsony 1996, Larsson et al. 2000). Gas particle densities $n(\text{H}_2)$ are found in the range from $\sim 10^4 \text{ cm}^{-3}$ to values larger than 10^6 cm^{-3} . Mass estimates based on the C^{18}O ($J = 1 - 0$) transition line give values of $\sim 250 - 300 M_\odot$ (McMullin et al. 2000, Olmi & Testi, 2002), while the C^{18}O ($J = 2 - 1$) line gives $\sim 1450 M_\odot$ (White et al. 1995). McMullin et al. (2000) argue that the estimate made on the $J = 1 - 0$ line is better than that based on $J = 2 - 1$ transition because the first is less sensitive to density and has a factor of 2-3 less opacity. Even allowing for larger uncertainties (but unrelated to the cloud distance), the difference seems to be significant and it is an open issue to be resolved. We remark

that the cloud mass is a key parameter in evaluating the star formation efficiency and the global star formation properties of the cloud.

The near-IR study of the dust properties by Eiroa & Hodapp (1989) showed that water ice absorption is widespread in the Serpens molecular cloud. They also detected solid CO absorption, further studied by Chiar et al. (1994), finding an unusually high ratio of CO to H₂O ice absorption. Ice features in the near- and mid-IR using Spitzer mid-IR spectroscopy and ground-based facilities have recently been studied by Knez et al. (2005), Pontoppidan et al. (2008), Boogert et al. (2008), and Öberg et al. (2008). The structure of the CO ice absorption has been studied by Pontoppidan et al. (2003b). Pontoppidan et al. (2003a) detected methanol in the wings of the 3.1 μm water ice feature in the lines of sight to SVS 4-2 and SVS 4-9, the first detection of the molecule toward low-luminosity young stars. Pontoppidan et al. (2004) subsequently extended the *L*-band observations to the whole SVS 4 stellar complex (Eiroa & Casali 1989). Big jumps in calculated extinction and water ice absorption were found from source to source, even over projected distances of only 10 arcseconds. Thus, some of the sources probably lie behind and some in front of an obscuring cloud, as well as being embedded in the envelope of the Class 0 SMM 4 object (Casali et al. 1993). The water ice optical depth-to-extinction ratio was used to infer abundances of 9×10^{-5} relative to H₂, corresponding to water ice mantle volumes around 40% of those in Taurus. In addition, it generally seems likely that methanol, with an abundance around 20% of that of water, is formed through grain-surface chemistry in pre-stellar low density conditions and cold temperatures ($T < 20\text{K}$), rather than in the gas phase. But the variation (detection) in abundance from source to source is puzzling and may indicate that the methanol formation is a transient phenomenon.

The ISOCAM CVF study of Alexander et al. (2003) extended mid-IR spectroscopy to 20 low-luminosity sources in Serpens. SVS 2 (the illuminating source of SRN) clearly shows the silicate feature in emission - see also Kessler-Silacci et al. (2006) for the 5-34 μm Spitzer spectrum. 12 other sources show deep absorption features. Water ice absorption at 6 μm is strong relative to silicate optical depth, compared to other regions. On the other hand, CO₂ absorption at 15.2 μm is weak in Serpens compared to silicate depth. The study shows clear differences in grain chemistry from region to region, perhaps related to age or other factors. Ciardi et al. (2005) have recently resolved the silicate feature in the binary SVS 20 and find that the mid-IR spectrum of each YSO is dominated by amorphous silicate emission with some crystalline silicates. Differences in the dust properties toward each component of the binary might be explained by their different luminosities.

4. The Embedded Population

Data obtained during the last 15 years in the infrared, submillimeter, millimeter, radio continuum and X-rays spectral domains reveal a dense, rich, young, low mass stellar cluster embedded in the Serpens core. More than 300 objects in all evolutionary phases, from collapsing gaseous condensations to Class II/III pre-main sequence (PMS) stars coexist within the $\sim 0.5 - 0.7$ pc Serpens central core. Fig. 4 shows an impressive colour composite from images taken through the near-IR bands *J*, *H* and *K* of the Serpens core. Individual images have 1 minute exposure each and were recently obtained during first light of the HAWK-I near-IR camera attached on UT4 of ESO's Very



Figure 4. The Serpens core and the embedded near-IR cluster seen in a J , H , and K composite image taken by the ESO's near-IR imager HAWK-I attached on UT4 of the VLT. The central object surrounded by an elliptical nebulous ring with spiral-like arms is the young binary SVS 20. At the top, the pre-main sequence star SVS 2 and its edge-on disk are clearly distinguished. The bottom of the image shows the SVS 4 sub-cluster. In addition, nebulous objects, H_2 emission knots, a widespread reflection nebulosity, and many YSOs are clearly seen.

Large Telescope. In the following, we review how the cluster appears at the different wavelength ranges.

4.1. The Near- and Mid-IR Cluster: Tracing the Class I, Flat-spectrum and Class II Object Population

Because of severe extinction, sensitive IR observations are required to sample the stellar population embedded in the Serpens core. Eiroa & Casali (1992), Horrobin et al. (1997), Sogawa et al. (1997), Giovannetti et al. (1998), Kaas (1999), Hodapp et al.

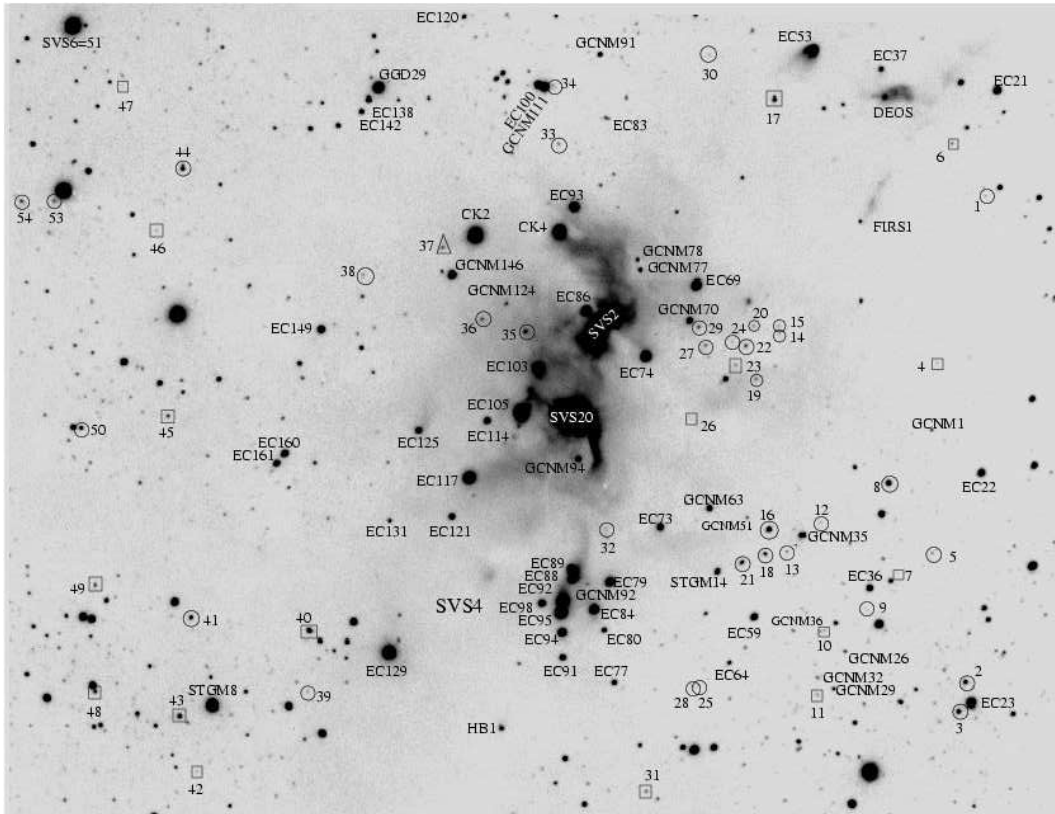


Figure 5. K -image of the Serpens core (size $\sim 8' \times 6'$). Some of the embedded objects are identified. Figure taken from Kaas (1999).

(1996), Hodapp (1999), have used near-IR cameras to study the young stellar population embedded in the core, within a region $\sim 10'$ approximately centred in SRN. The achieved sensitivity is $K \sim 15 - 16.5$ mag. The images reveal a relatively large diffuse reflection nebula, about $2' \times 3'$ in size, in the center of the core, extending from the optical SRN towards the South up to the position of the SVS 4 complex (Strom et al. 1976, Eiroa & Casali 1989), some nebulous objects and knots, and a large number of red stellar objects, which are not visible in optical wavelengths (even up to $0.9 \mu\text{m}$, e.g. Gómez de Castro et al. 1987, Giovannetti et al. 1998). A variety of criteria has been used to identify near-IR embedded objects, e.g. near-IR excesses, variability, association with nebulosity. Fig. 5 reproduces the K -band image from Kaas (1999) where many YSOs are indicated. Table 1 gives names, J2000 equatorial coordinates, and JHK magnitudes of the (up to now) identified near-IR (JHK) YSOs. The table includes objects from the aforementioned works, as well as from other references. Further, by compiling the table, we have observed that some objects show a non-negligible brightness difference ($\Delta K > 0.5$) between different studies; these objects most likely belong to the young cluster and are therefore included in the table. A few of the objects listed in the table are located outside the Serpens central core; we have chosen to

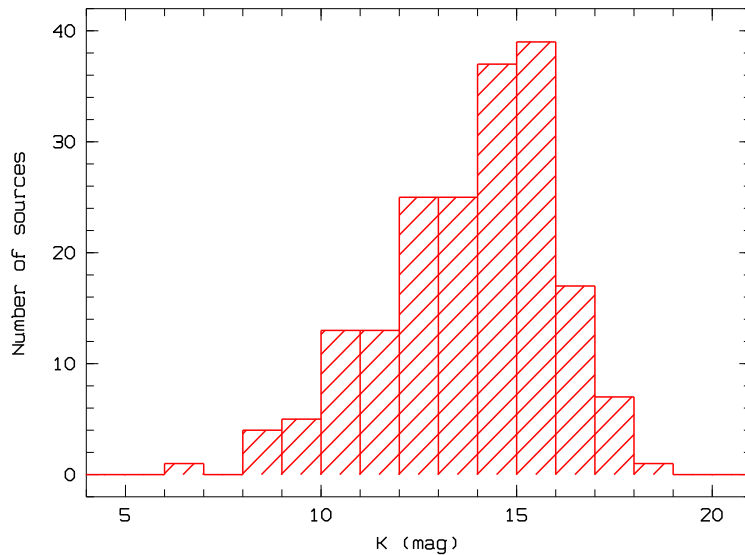


Figure 6. K histogram of the near-IR Serpens objects.

include them for completeness. Klotz et al. (2004) have recently conducted a deeper (K completeness limit ~ 19 mag.) near-IR survey in a region $5' \times 10'$ in size. This work differs from the others because the observed area lies towards the SW from SRN, in a region where the obscuration is obviously smaller than in the core center (see Fig. 1 and 6 of Klotz et al. 2004). Klotz et al. suggest 14 further candidates as Serpens members, from which three may be brown dwarfs. These objects are also included in Table 1. Using Spitzer and Chandra data Winston et al. (2007) have identified more than 100 YSOs in Serpens; some of them have 2MASS counterparts. These 2MASS objects are included in Table 1 although some of them are also located outside the central gaseous/dusty core. Thus, the total number of identified near-IR Serpens object candidates in the central core or close to it is 252. The near-IR sources are distributed across the whole Serpens core, although there is a clear concentration towards the SE clump, either embedded in the near-IR nebula or relatively close to it (see Sect. 5).

Many of the Serpens objects appear to be binaries or forming part of small sub-clusters. The SVS 4 complex is the outstanding case, where ~ 10 objects appear to form a compact group, embedded in a common faint nebulosity spread over a field $\sim 35'' \times 35''$ in size. SVS 20 is an example of a binary with interesting properties (see Sect. 8 for a more detailed description of SVS 4 and SVS 20). Haisch et al. (2002, 2004) and Duchêne et al. (2007) have found a multiplicity fraction of $\sim 35\%$ in a limited sample of Serpens Class I/flat-spectrum sources.

Fig. 6 provides the histogram of the apparent K magnitude of the Serpens objects. The number of sources increases up to the sensitivity limit of the near-IR surveys, supporting the suggestion of Kaas (1999), and contradicting the presence of a turnover in the luminosity, as suggested earlier by Eiroa & Casali (1992) and Giovannetti et al. (1998). The histogram in Fig. 6 does not reflect the true luminosity and mass functions of the Serpens near-IR cluster since magnitudes are not corrected for extinction, but it

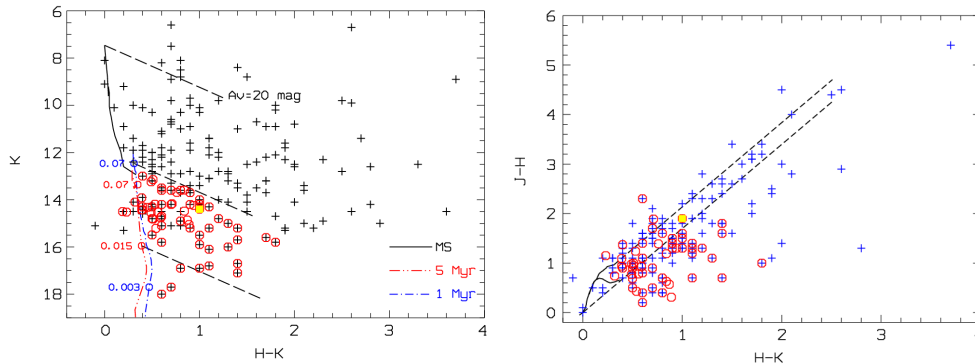


Figure 7. Left: Colour-magnitude diagrams of the Serpens objects. The continuous line represents main-sequence stars, while dashed-dotted lines are 1 Myr (blue colour) and 5 Myr (red colour) isochrones from Baraffe et al. (2003). Dashed lines represent reddening vectors, $A_V = 20$ mag. K -magnitudes have been scaled to a distance of 230 pc. Right: Colour-colour diagram of the Serpens objects. The continuous line represents main-sequence and giant stars while dashed lines are reddening vectors. Squares (red colour) in both diagrams are brown dwarf candidates (see text); the confirmed Serpens brown dwarf is represented by the filled square (yellow colour).

does show that a non-negligible number of Serpens objects are intrinsically very faint, and consequently very low-mass YSOs (see below and Sect. 6). Fig. 7 reproduces the colour-magnitude ($H - K$, K) and colour-colour ($H - K$, $J - H$) diagrams of the sources. Some objects are located in an “anomalous” position towards the left of the main-sequence line. This is likely due to source variability (photometry was not always obtained simultaneously), binarity, and/or scattering which can yield a blueing in $H - K$ colour (for the most extreme case, SVS 1, see the comments by Kaas 1999). Many sources present an excess or lie along the reddening line with large extinction values. The colour-magnitude diagram suggests that some of the sources must be reddened, young, very low mass M stars and/or brown dwarfs, since in the colour-magnitude diagrams they are located in the area where substellar objects are expected. These brown dwarf candidates are identified in Table 1. EC 64 (GCNM 57, BD-Ser1) was identified as a young L0-L3 brown dwarf by Lodieu et al. (2002) and two more brown dwarf candidates have been suggested by Klotz et al. (2004). Winston et al. (2007) suggest objects with $m_K > 12.5$ as brown dwarfs candidates. In addition, Kaas et al. (2004) suggest a few brown dwarf candidates among the Serpens objects on the basis of ISO data and the estimated low, bolometric nebulosity ($L_{bol} \leq 0.04L_{\odot}$).

Near-IR spectra of some objects have been taken by Aspin et al. (1994), Casali & Eiroa (1996a), Preibisch (1999), Hodapp (1999), Doppmann et al. (2005), Covey et al. (2006), Aspin & Greene (2007), Eiroa et al. (2008). Fig. 8 shows some representative K -spectra. The spectra usually show atomic absorption lines, e.g. NaI, CaI, as well as CO absorption bands, which correspond to late K and M spectral types, similar to Classical T Tauri stars. (As noted above, there is a brown dwarf spectroscopically confirmed by Lodieu et al. 2002). In some cases, the atomic and molecular bands appear in emission, most likely due to circumstellar disks; in addition, the spectra of some objects appear to be veiled by dust emission and are flat. The spectroscopic and photometric data suggest that the near-IR is mainly tracing the Class II population of

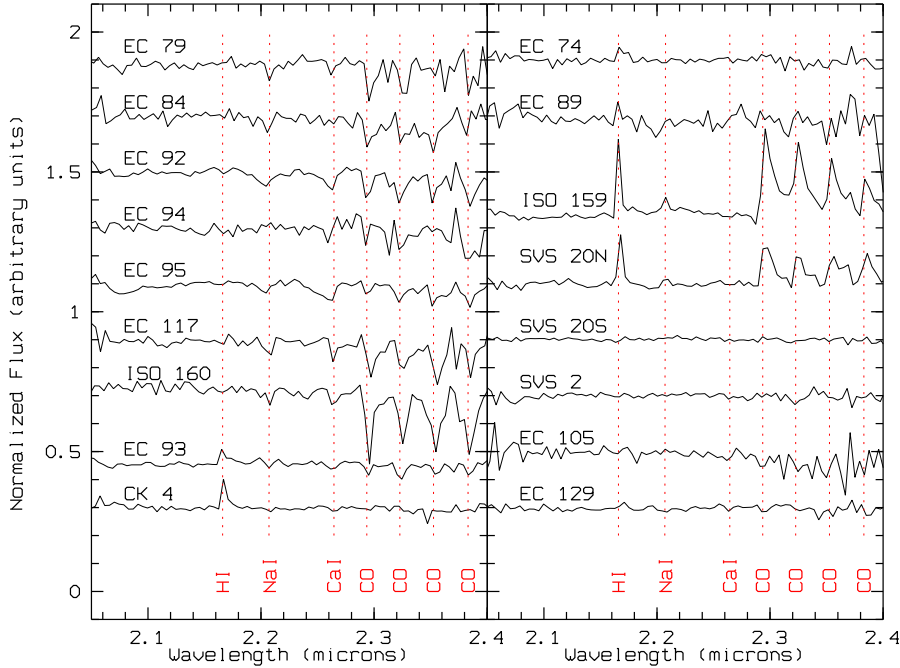


Figure 8. Near-IR spectra of some Serpens objects, including Class II, flat-spectrum and Class I sources (Eiroa & Djupvik, unpublished).

the Serpens cluster. We note, however, that some flat-spectrum and Class I sources are detected in the near-IR (Kaas et al. 2004, Harvey et al. 2007a, Winston et al. 2007, see next paragraph) and show photospheric lines (e.g. Doppmann et al. 2005); even further, near-IR counterparts of very young Class 0 sources have been suggested by Hodapp (1999, see also Eiroa et al., 2005).

Serpens was observed within the ISO central programme in two filters centred at 6.7 and 14 μm . 0.13 square degrees were covered by three overlapping maps, one centred in the core, a second one towards the West, and a third one towards the South (Kaas et al. 2004). A total of 421 sources were detected, out of which 392 sources were found at 6.7 μm , 140 at 14 μm , and 124 at both wavelengths. ISO is particularly useful to detect young sources with no near-IR excess but with a distinct mid-IR excess. On the basis of the spectral index α_{IR}^{7-14} the ISO sources separate into two distinct groups: “red” sources with IR excess (53 objects), which are YSOs surrounded by circumstellar dust, and “blue” sources (71 objects), which likely are field stars, although some of them could be Serpens Class III objects. Using ISO data and near-IR data Kaas et al. (2004) identify 20 Class I and 13 flat-spectrum protostars, and 43 Class II stars (i.e. embedded CTTs) among all the ISO sources. Serpens is one of the star formation regions observed by the c2d Spitzer project (Evans et al. 2003). The Spitzer/IRAC and MIPS observations extend to a large region (Harvey et al. 2006, 2007a, 2007b, see below). The young stellar population of the core, called Cluster A by Harvey and collaborators, is included in the analysis of the whole Serpens cloud by Harvey et al., while Winston et al. (2007) specifically analyze the Spitzer core data, extending their

work to a region a bit larger than the dense central core. Fig. 9 shows a three colour, 4.5, 8.0 and 24 μm Spitzer image of the core (Harvey et al. 2007a). By using Spitzer data, 2MASS, and Chandra observations, Winston et al. (2007) identify 229 Serpens candidate objects, out of which 138 are considered bona fide YSOs: 22 Class 0/I protostars, 16 flat-spectrum sources, 62 Class II stars, 17 transition disk candidates, and 21 Class III sources. The relative number of ISO and Spitzer Class 0/I to Class II sources in Serpens is considerably larger than in similar young clusters, like ρ Oph, Chamaeleon or Taurus; in fact, the number fraction Class I/Class II in the core is almost 10 times higher than 'normal' (Kaas et al. 2004, Schmeja et al. 2005, see Winston et al. 2007 for a comparison with other regions observed in the context of the c2d project), which indicates that the embedded population is extremely young and active.

Spitzer IRS spectra of five Serpens objects (EC 74, EC 82, EC 90, EC 92, and CK 4) have been studied by Lahuis et al. (2007). They detected H_2 S(2) and [NeII] emission towards EC 74, EC 82 and EC 92, indicative of a significant hot gas component in the disks ($T > 500$ K) and a [NeII] excitation mechanism through X-Rays or EUV.

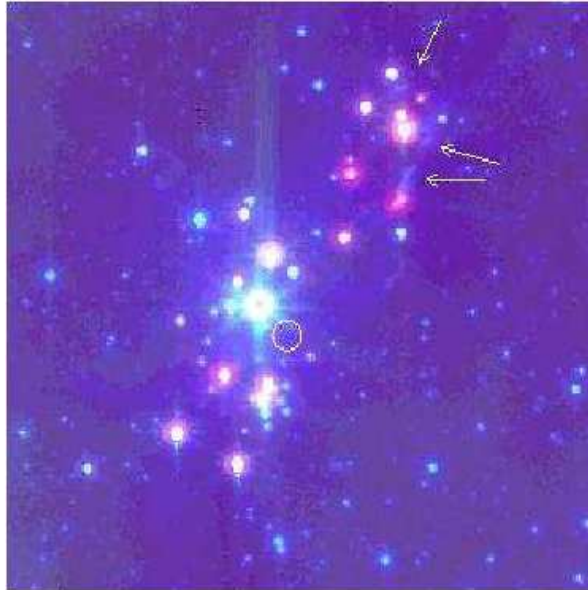


Figure 9. Three-colour Spitzer image of the Serpens core. Colour coding is: blue/4.5 μm , green/8.0 μm , and red/24 μm . Image taken from Harvey et al. (2007a).

4.2. The Submillimeter and Millimeter Cluster: Tracing the Class 0 and Pre-stellar Population

About a dozen of discrete sources embedded in the cloud core have been found by submm observations (Casali et al. 1993, White et al. 1995, Reipurth et al. 1996, Davis et al. 1999, Enoch et al. 2007, Wu et al. 2007). Fig. 10 shows the submm maps at 850 and 450 μm of the core, after Davis et al. (1999). Several sources - SMM 1, SMM 5, SMM 6, SMM 9, SMM 10 - have been identified with near-IR and ISO/Spitzer sources (Casali et al. 1993, Hodapp 1999, Kaas et al. 2004, Winston et al. 2007) and some of them - SMM 2, SMM 3, SMM 4 - with IRAS and ISO far-IR sources (Hurt &

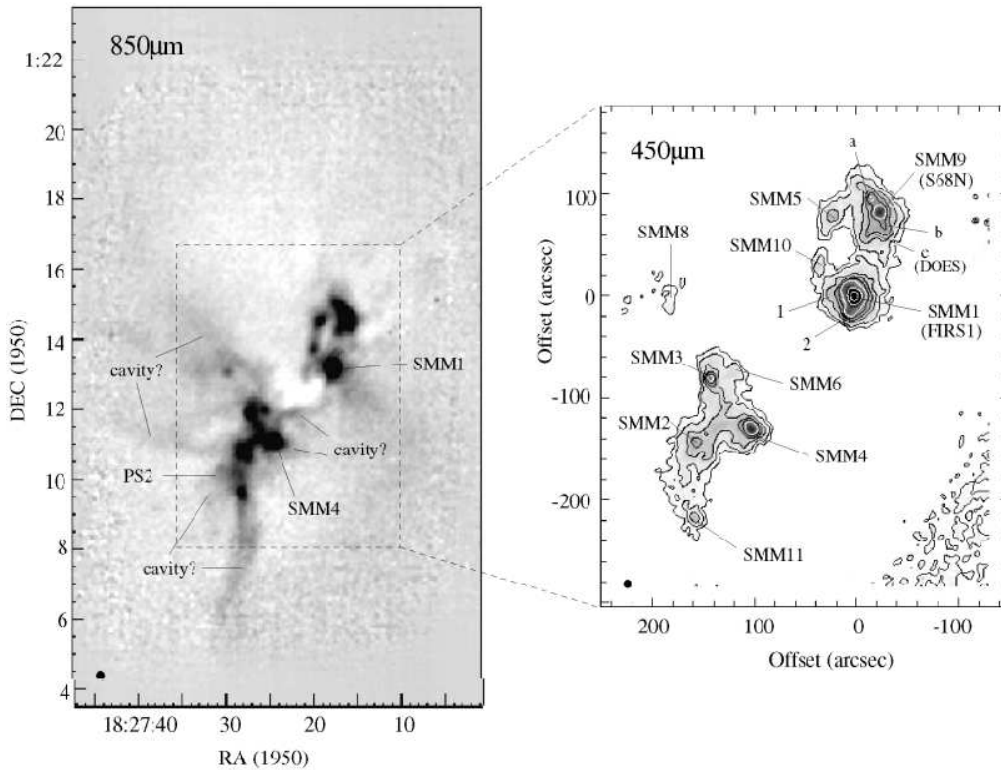


Figure 10. Submillimeter images of the Serpens core. Figure taken from Davis et al. (1999).

Barsony 1996, Larsson et al. 2000). An analysis of their SEDs shows that they form a cluster of very young, low to intermediate luminosity Class 0 objects (or borderline Class 0/Class I objects), with dust temperatures in the range $\sim 20 - 50 K$ (Casali et al. 1993, McMullin et al. 1994, 2000, Hurt & Barsony 1996, Wolf-Chase et al. 1998, Davis et al. 1999). Some sources have been modelled in terms of a stellar core, an accretion disk and an extended, massive envelope (Hogerheijde et al. 1999, Brown et al. 2000, Larsson et al. 2000). Kinematic infall signatures have been suggested for a number of the submm sources - SMM 2, SMM 3, SMM 4, SMM 9 (Hurt et al. 1996, Gregersen et al. 1997, Mardones et al. 1997, Williams & Myers 2000, Narayanan et al. 2002), although at least in the case of SMM 9 (S 68N) this interpretation is controversial (Wolf-Chase et al. 1998).

Interferometric observations at 3 mm carried out by Testi & Sargent (1998) reveal 32 discrete sources widespread in the cloud core (Fig. 11), and 26 out of 32 are probably protostellar continuum condensations, with masses in the range $0.3 - 5.0 M_{\odot}$. The sources are distributed into two groups: the more numerous is associated with the NW core clump and the second one with the SE clump. Seven of the 3 mm sources in the NW clump are also detected by Williams & Myers (2000). These authors also find 8 gaseous (CS and N_2H^+) condensations in the NW clump, with high peak temperatures and low velocity dispersion, 6 of which without associated continuum sources. These quiescent cores have typical sizes of 5000 AU and display spectra indicative of infalling

motions; they are suggested to be pre-protostellar collapsing cores. A further turbulent, contracting, starless core was also found towards the West of S 68N by Williams & Myers (1999). Recently, SMM 1 has been observed at 1.3 and 3.3 mm with the PdB interferometer (Fuente et al. 2007).

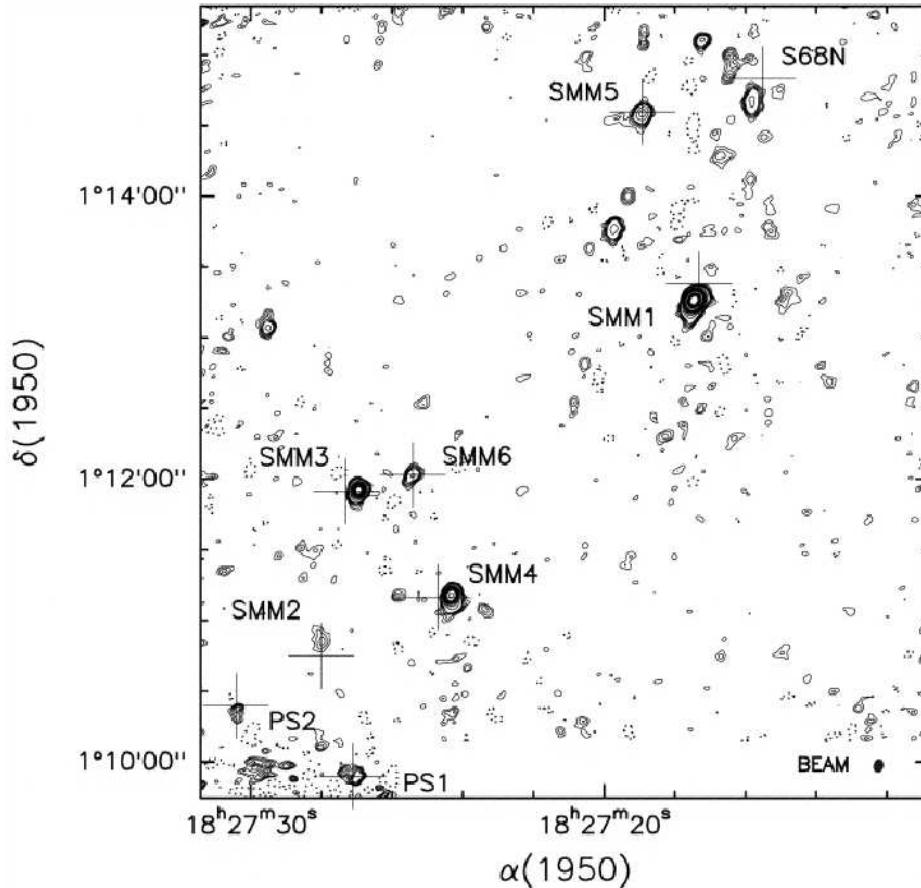


Figure 11. 3 mm continuum image from the Serpens core. The positions of some submm sources and far-IR sources (PS1 and PS2) are indicated. Figure taken from Testi & Sargent (1998).

4.3. Radio Continuum Observations

Very few observations of the core have been made in the centimeter radio continuum (Rodríguez et al. 1980, 1989, Ungerechts & Güsten 1984, Snell & Bally 1986). FIRS 1 is the only source with detailed studies due to its unique radio properties (see Sect. 8). Smith et al. (1999) report several VLA sources in the region around the SVS 4 complex. Recently, Eiroa et al. (2005) have analysed 3.5 cm VLA data of the whole Serpens core. They find 22 radio continuum sources, 16 of which seem to be associated with YSOs. The radio sources are distributed into two groups: one associated with Class 0/Class I sources in the NW clump of the core, and a second one towards the SE clump, where the radio continuum sources are associated with all kind of objects - from Class 0 to Class

II sources. It is likely that the radio emission from the Serpens objects is produced by thermal jets, but the radio emission of some sources in the SE clump likely originates in coronally active PMS stars as suggested by Smith et al. (1999, see also Preibisch 2003, Eiroa et al. 2005). Further observations to estimate radio spectral indexes of the sources as well as their sub-arcsec structure would be very useful to determine the nature of the Serpens radio continuum objects. Recently, Forbrich et al. (2007) have searched for coronal radio emission from EC 95 using VLBI with a non-detection result.

4.4. X-ray Observations

X-ray emission has been studied by Preibisch (1998, 1999, 2003, 2004) using ROSAT and XMM. ROSAT detected very strong X-Ray emission associated with the flat-spectrum source EC 95, one of the stars in the SVS 4 group (Sect. 8). XMM observations have detected ~ 50 sources in a field $\approx 30'$, several of them associated with YSOs. Among the X-ray sources, 4 are associated with Class I protostars, two with flat-spectrum sources, and at least 9 with Class II objects. X-ray Class I protostars are among the brighter Serpens Class I objects in the K -band, which could mean that these YSOs have higher bolometric luminosities and/or suffer less extinction than the X-ray undetected Class I objects. The X-ray Class I objects present a strong flare-like variability, with flare frequency a factor two higher than the flare frequency in typical T Tauri stars, although the Class II object EC74 shows a large variability in its X-ray luminosity (a factor of 10). The X-ray emission of Class I protostars is suggested to be due to the magnetic coupling between the protostars and their circumstellar disks. The X-ray emission of Class II objects is normally ascribed to magnetic dynamo processes in the stellar coronae of the PMS stars. We point out that 4 of the X-ray sources have VLA counterparts: the Class I object EC 53, the flat-spectrum source SVS 20, and the Class II sources EC 95 and EC 117.

A deep Chandra X-ray survey has been carried out by Giardino et al. (2007), with the aim to determine whether Class 0 protostars emit X-rays. A total of 85 X-ray sources are detected, none associated with Class 0 objects. The light curves and spectra of 35 YSOs are derived. These authors find a trend of decreasing absorbing column densities from Class I to Class III sources, and some evidence of decreasing

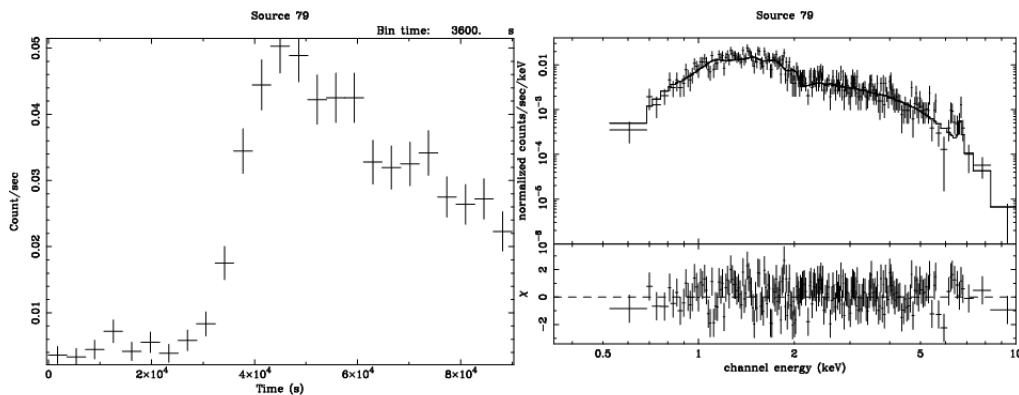


Figure 12. Light curve and spectra with spectral fit of the Class II object Chandra 79 (Giardino et al. 2007).

plasma temperatures. The Chandra source 79 (ISO 393, a Class II source) underwent a large, long duration flare (Fig. 12) for which Giardino et al. (2007) derive a semi-loop length $L = 10 - 12R_{\odot}$, and suggest that the long flaring loop could be explained if the flare is due to a magnetic reconnection event of a flux tube linking the star's photosphere with the inner ring of a circumstellar disk. The spectrum of this YSO shows 6.4 keV Fe fluorescent emission compatible with reflection off a circumstellar disk irradiated by the hard X-ray continuum emission of the flare. Using the Chandra data, Winston et al. (2007) find that 60 YSOs have detectable X-ray emission: 9 of the X-ray sources are associated with Class I objects, 8 with flat-spectrum sources, 21 have Class II counterparts, 2 are transition disks. Twenty Class III sources are identified solely by their X-ray emission. Comparing with the relative numbers of Serpens YSOs in each evolutionary class, there appears to be no evidence of a trend in the detection rate of sources by class.

4.5. Outflows and Masers

Low spatial resolution observations by Bally & Lada (1983) detected a very large, $\sim 12' \times 17'$, CO outflow with both blueshifted and redshifted components approximately centred in SRN, which could not be ascribed to a single driven source. Higher resolution CO observations show widespread high velocity gas that extends over the core and resolved, molecular outflows associated with Class 0 and Class I YSOs (White et al. 1995, also Eiroa et al. 1992, Davis et al. 1999). NH_3 , SiO, CS, HCO^+ , HCN compact outflows are associated with FIRS 1 (SMM 1), S 68N (SMM 9), SMM 3, SMM 4 and SMM 10 (Torrelles et al. 1992, McMullin et al. 1994, Curiel et al. 1996, Wolf-Chase et al. 1998, Hogerheijde et al. 1999, Williams & Myers 2000). It is interesting to note that some of these sources also show infall signatures (Sect. 4.2).

An H_2 jet with a point-like object (EC 41) at its apex close to the position of FIRS 1/SMM 1 was detected by Eiroa & Casali (1989, see also Rodríguez et al. 1989), although the relationship between the H_2 emission and the Class 0 object was unclear. Later studies (Curiel et al. 1996, Hodapp 1999) show that they more likely are unrelated objects and the H_2 jet is not driven by the Class 0 object which, on the other hand, is powering radio molecular line outflows, and a radio continuum jet (see Sect. 8). H_2 knots and jets widely distributed in the cloud core were detected by Herbst et al (1997, these authors provide equatorial coordinates of many H_2 condensations), Eiroa et al. (1997b) and Caratti o Garatti et al. (2006). Hodapp (1999) studied the proper motions of the jets located in the NW core clump; Fig. 13 shows these results. The H_2 emission has been associated with Class 0, Class I, flat-spectrum and Class II objects - SMM 3, SMM 4, SMM 9, GCNM 53 (ISO 276), EC 37, SVS 20 and EC 105. There is some ambiguity in certain cases, e.g. a jet could be associated with either the Class 0 object SMM 3 or the Class II source EC 105. Spectral imaging in H_2 using ISO-CAM-CVF data of the Serpens core have been presented by Larsson et al. (2002). These authors also present ISO-LWS maps of several forbidden lines in the far-IR.

GGD 29 was proposed as a suspected Herbig-Haro object by Gyulbudaghian et al. (1978), although later observations showed it to be a reflection nebulosity with a young star at its apex (Hartigan & Lada 1985, Warren-Smith et al. 1987). Thus, the first confirmed Herbig-Haro objects in the Serpens molecular cloud, HH 106/107 and HH 108/109, were discovered by Reipurth & Eiroa (1992). HH 106 and HH 107 are located towards the West and North of the central core (see e.g. Fig. 2 by Ziener & Eislöffel 1999). The emission line star ESO $\text{H}\alpha$ 279a (IRAS 18296+0116), located between

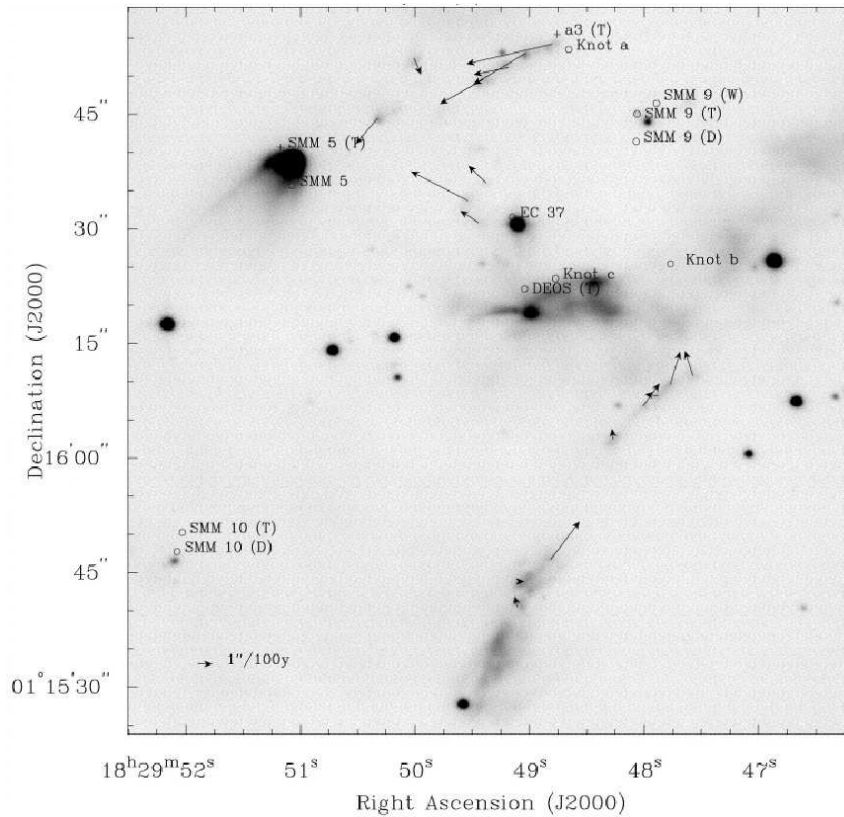


Figure 13. Proper motion vectors of H₂ emission knots in the NW clump of the Serpens core. Figure after Hodapp (1999).

both HH objects, has been suggested as the exciting source of a large bipolar flow with both HH 106 and HH 107 at its opposite ends (Aspin et al. 1994, Chini et al. 1997). HH 108/109 are located $\sim 2.3^\circ$ SE from the central core and likely are excited by the Class I object HH 108 IRAS/VLA 1, close to the Class 0 object HH 108 MMS (Chini et al. 1997, 2001, Siebenmorgen & Krügel 2000, Reipurth et al. 2004, Connelley et al. 2007). Gómez de Castro (1997) detected spectroscopically an HH condensation $88''$ eastwards from SVS 2, the exciting source of SRN. In addition, deep CCD H α and [SII] images of the core (Davis et al. 1999) and of a 3.15 square degrees of the large scale cloud (Ziener & Eislöffel 1999) have revealed many HH condensations, most of them concentrated in the core; Ziener & Eislöffel (1999) give equatorial coordinates of 29 HH objects and condensations. Fig. 14 shows some examples of HH objects in the Serpens core. Potential exciting sources of the HH objects have been suggested, e.g. FIRS1/SMM 1, EC 105, EC 92 and EC 117. Finally, HH 476 is located close to the emission line star group Ser G3-G6 (Cohen & Kuhl 1979, Ziener & Eislöffel 1999).

OH maser emission associated with FIRS 1 was detected by Rodríguez et al. (1989, see also Clark & Turner 1987, Mirabel et al. 1987). H₂O maser emission associated with FIRS 1 and S 68N has been observed by several groups (Blair et al. 1978, Rodríguez et al. 1978, 1980, Dinger & Dickinson 1980, Palla & Giovanardi 1989, Curiel et al. 1993, Wolf-Chase et al. 1998). Furuya et al. (2003) detected H₂O

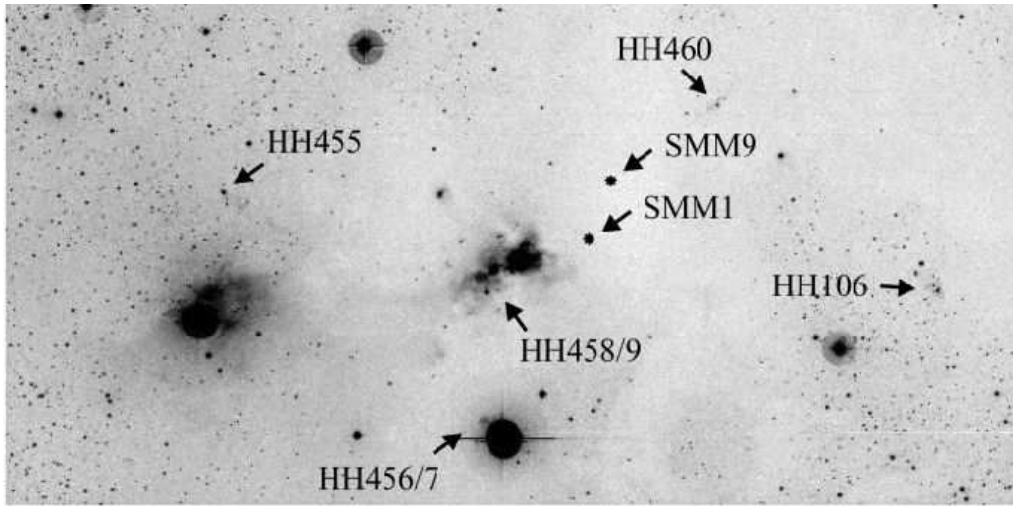


Figure 14. Some examples of HH objects in the Serpens core. Figure after Davis et al. (1999).

maser emission towards several Serpens Class 0 sources; and recently Moscadelli et al. (2006) have carried out a detailed study of the spatial distribution and proper motions of the FIRS 1 H₂O maser, which is formed by two small clusters of features.

5. Spatial Distribution of YSOs in the Core

Eiroa & Casali (1992) noticed that the Serpens near-IR sources are concentrated towards the core. A more detailed analysis of the spatial distribution of Serpens YSOs has been made by Testi et al. (2000), Kaas et al. (2004), Harvey et al. (2007a), Enoch et al. (2007), and Winston et al. (2007). The distribution shows a remarkable subclustering, with the youngest sources mainly concentrated towards the NW and SE core clumps, which is seen by Testi et al. (2000) as an observational support for hierarchical fragmentation within a cluster-forming core. The spatial distribution of the Serpens YSO core cluster is shown in detail in Fig. 15, where we plot the distribution of the sources grouped according to their evolutionary class. Table 2 gives a cross-correlation of the sources detected in the different wavelength regimes and their evolutionary classes. The near-IR cluster members are seen across the whole core, although their number is clearly smaller towards the field around FIRS 1 and S 68N in the NW clump; brown dwarf candidates follow this distribution. Most of the near-IR sources likely are Class II objects, although few of them are associated with the youngest Class I and Class 0 objects (Sect. 4.1). The embedded Class II population detected with ISO/Spitzer is also seen across the whole core, although predominantly towards the densest part of the core and more accentuated towards the SE clump. Class I, Class 0 and mm cores are exclusively seen towards the densest parts of the two core clumps (with only one exception). There are approximately the same number of Class I and Class 0 objects in each of the NW and SE clumps, but the number of mm cores is clearly larger towards the NW clump, which is the opposite of the spatial distribution for the near-IR and ISO

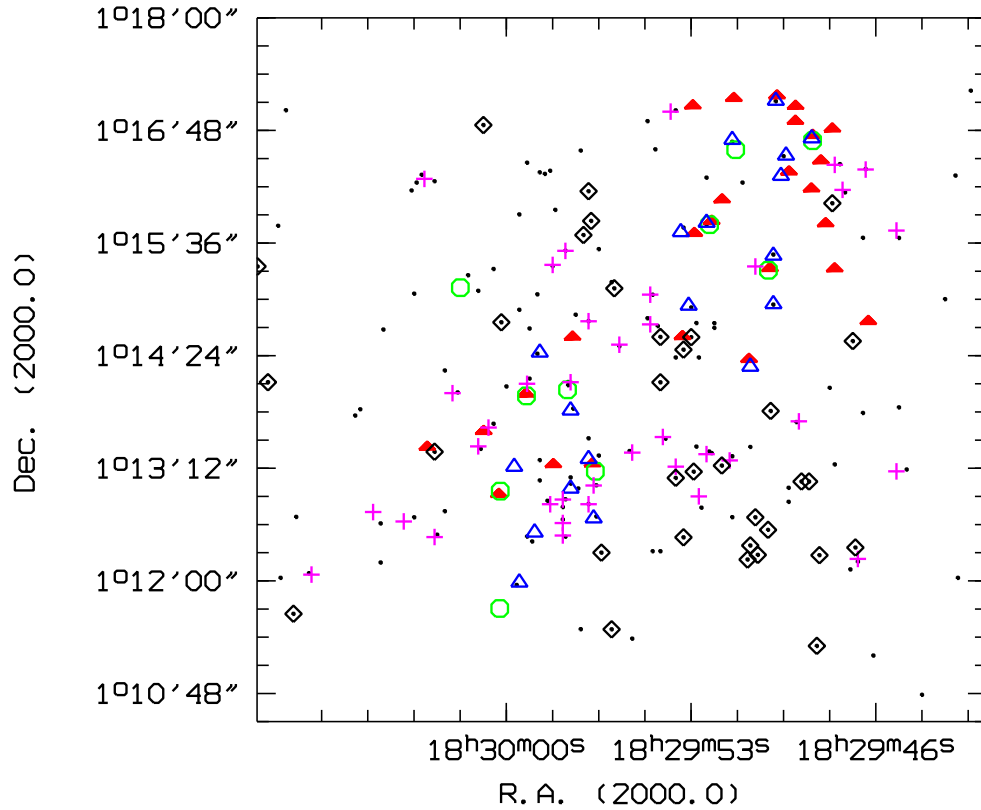


Figure 15. Spatial distribution of YSOs in the Serpens cloud core. The plotted area approximately corresponds to that observed by Testi et al. (1998, see our Fig 11). Symbols mean the following: dots (black): near-IR sources; crosses (magenta): Class II ISO sources; open triangles (blue): Class I ISO sources; open hexagons (green): Class 0 sources; filled triangles (red): mm cores; diamond (black): brown dwarf candidates.

Class II sources. These results suggest that star formation activity is currently taking place in both core clumps, but is more active in the NW one, while it was more efficient or began earlier in the SE one. It is interesting to recall that both clumps are clearly distinct as indicated by their kinematics (Testi et al. 2000). These authors and Kaas et al. (2004) estimate the mean stellar/protostellar density of the Serpens core in the range of $\sim 1000 \text{ pc}^{-3}$, and is even larger, several thousands, in localized subclusters (Eiroa & Casali 1989, Testi et al. 2000). This high stellar density is hardly exceeded by any other star formation region, specially if the youngest Class 0 and mm cores are considered (Kaas et al. 2004, Testi et al. 2000). Winston et al. (2007) find that the projected spacing of Class 0/I sources is only 5000 AU, similar to the Jeans's length and the radii of critical Bonnor-Ebert spheres; they suggest that the volumes of gas from which these objects accrete may overlap and competitive accretion could be taking place. Collisions

between protostellar envelopes may be common, which could explain the widespread high velocity gas and overlapping outflow lobes (White et al. 1995)

6. Luminosity and Mass Functions

Intrinsic luminosity functions in young stellar clusters are usually based on near-IR magnitude distributions; their evaluation is not simple because one has to deal with extinction estimates, variability and the contribution of accretion disks to the observed magnitudes. Eiroa & Casali (1992) and Giovannetti et al. (1998) first estimated a luminosity function on the basis of K -band magnitudes. A likely more reliable luminosity function of Serpens ISO Class II objects has been produced by Kaas et al. (2004). These authors compare their estimated Class II luminosity function to pre-main sequence evolutionary models and find that the Class II population is compatible with coeval formation about 2 Myrs ago and a three-segment power-law initial mass function, similar to other clusters like ρ Ophiuchi. Harvey et al (2007a) find for all clusters in the whole Serpens cloud (see next section) that the luminosity function peaks around a few times $10^{-2} L_{\odot}$ and drops to both lower and higher luminosities. Testi & Sargent (1998) find that the mass-spectrum of the 3 mm continuum sources is consistent with a stellar initial mass function, supporting the idea that fragmentation of cloud cores determines the stellar masses. Considering the masses of the different objects embedded in the Serpens core, the star formation efficiency has been estimated to be of the order of ~ 3 -10 %, although higher figures are likely in the densest parts of the core clumps (Olm & Testi 2000, Kaas et al. 2004). In addition, since the mm objects as well as the Class 0 and Class I protostars are not older than $\sim 10^5$ years, their coexistence in the cloud core with the younger Class II and near-IR cluster suggests that star formation has proceeded in several phases (Casali et al. 1993, Kaas et al. 2004), but see Testi et al. (2000) for an opposite view.

7. Other Sites of Active Star Formation in the Serpens Cloud

As already pointed out (Sect. 1) relatively few works have studied the Serpens cloud outside the dense core, although different sites are known in which active star formation is taking place, e.g., Clark (1991) identified IRAS sources close to dense molecular material, and the ISOCAM data of Kaas et al. (2004) detect some mid-IR excess sources located several arcminutes south from the Serpens core.

The Herbig-Haro objects HH 108-109, located $\sim 2.3^{\circ}$ South-East from the core (Reipurth & Eiroa 1992, Ziener & Eislöffel 1999), form a bipolar outflow excited by the Class 0/I source IRAS 18331-0035, which is seen at cm wavelengths as a subarc-sec radio jet (Reipurth et al. 2004). The IRAS source was detected at 1.3 mm by Chini et al. (1997), as well as a second, very cold object called HH 108 MMS; images at mm/submm wavelengths by Chini et al. (2001) show an emission bridge linking both sources. HH 108 MMS has only been detected in the FIR and mm/submm in emission (Chini et al. 2001) and in absorption at $14 \mu\text{m}$ against a diffuse background (Siebenmorgen & Krügel 2000). A second absorbing core, Q1, at $14 \mu\text{m}$ is also detected. HH 108 MMS is suggested to be an extremely young protostellar source either on the verge of collapse or just beginning the protostellar phase (Chini et al. 2001).

Chavarría et al. (1988) and de Lara et al. (1991) carried out a photometric and spectroscopic study of several intermediate mass stars associated with nebulosity, including the Herbig Ae star VV Ser. They also identified 13 probable H α emission stars. Cohen & Kuhi (1979) found a close group of 4 optically visible T-Tauri stars, which they called Ser/G3-G6, about 45' to the south of the SRN (see Fig. 1).

The area around Ser/G3-G6 was mapped in the ammonia 1,1 emission line by Clark (1990, 1991) who found an NH₃ core on each side of the complex, Ser/G3-6ne and Ser/G3-6sw; HH 476 is close to the Ser/G3-6sw core (Ziener & Eislöffel 1999). Those authors point out that IRAS 18263+0027 and IRAS 18265+0028 are within about 1 and 2 arcminutes from the Herbig-Haro object, respectively, but consider it more likely that its exciting source is one of the stars in the Ser/G3-G6 complex. Wu et al. (2002), on the other hand, identify IRAS 18265+0028 as the energy source of HH 476; a H₂O maser has been detected by Persi et al. (1994) at the position of this IRAS source. A survey at 6.7 and 14.3 μm with ISOCAM in a 17' \times 19' field centred on Ser/G3-G6 reveals a cluster of about 40 IR excess sources out of 186 detections (Djupvik et al. 2006). This population consists mainly of Class II sources, but also a handful of Class I sources. Deep follow-up imaging in the 2.122 μm 1-0 S(1) line of H₂ centred on the Ser/G3-6ne NH₃ core shows a number of knots and jets not seen in the optical. At the position of IRAS 18265+0028 there are two red and bright sources, ISO-NH3-90 and 94, which probably are Class I/Class 0 type YSOs. In addition, ISO-NH3-101 is a red source with apparent excess emission at 6.7 μm , probably indicating H₂ line emission in this band.

Within the Legacy project *From Molecular Cores to Planet-Forming Disks* (c2d) of the Spitzer Space Telescope (Evans et al. 2003), a 0.9 deg² area in Serpens has been surveyed with IRAC and MIPS. A region about 2 degrees in DEC and 40 arc minutes in RA has been mapped in the 4 IRAC bands (3.6, 4.5, 5.8, and 8.0 μm) and the 3 MIPS bands (24, 70 and 160 μm), the MIPS scans being some 20% larger than the IRAC scans. This area was chosen to follow the $A_V = 6$ mag contour in the extinction map of Cambrésy (1999). Fig. 16 shows a composite image made from IRAC1, IRAC2, and IRAC4 filter. The map includes both the Cloud Core (Cluster A), the Ser/G3-G6 complex (Cluster B), and the region around VV Ser (Cluster C), to mention some known objects. Spitzer/IRAC reveals more than 250 Serpens sources distributed into the three mentioned areas (Harvey et al. 2006, Harvey et al. 2007a). This latter work presents detailed SEDs of the YSO objects in the whole area observed by Spitzer, traces the YSO luminosity function down to a limit of $\sim 10^{-3} L_{\odot}$, and shows the spatial clustering of the young objects according to their evolutionary classification. They also provide a table of Spitzer objects with counterparts at other wavelength ranges. Flaherty et al. (2007) have studied the infrared extinction law in the IRAC bands and the 24 μm MIPS band. The extinction law is similar to that of other regions but it differs from the diffuse ISM, which could be due to different dust properties. In addition, Harvey et al. (2007b) find a close correlation between the coolest dust detected at 160 μm and the dust associated with optical extinction. The region observed by Spitzer has been mapped at 1.1 mm by Enoch et al. (2007). They find 35 sources, most of them located in the Cluster A and Cluster B (Fig. 17). Those authors correlate the mm emission with the extinction map and find that most of the mm sources lie within regions of high extinction ($A_V > 10$ mag).

In the context of the Spitzer Gould Belt Legacy Survey, a new young embedded cluster (Fig. 18) associated with a filamentary dark cloud, located 3° to the South of

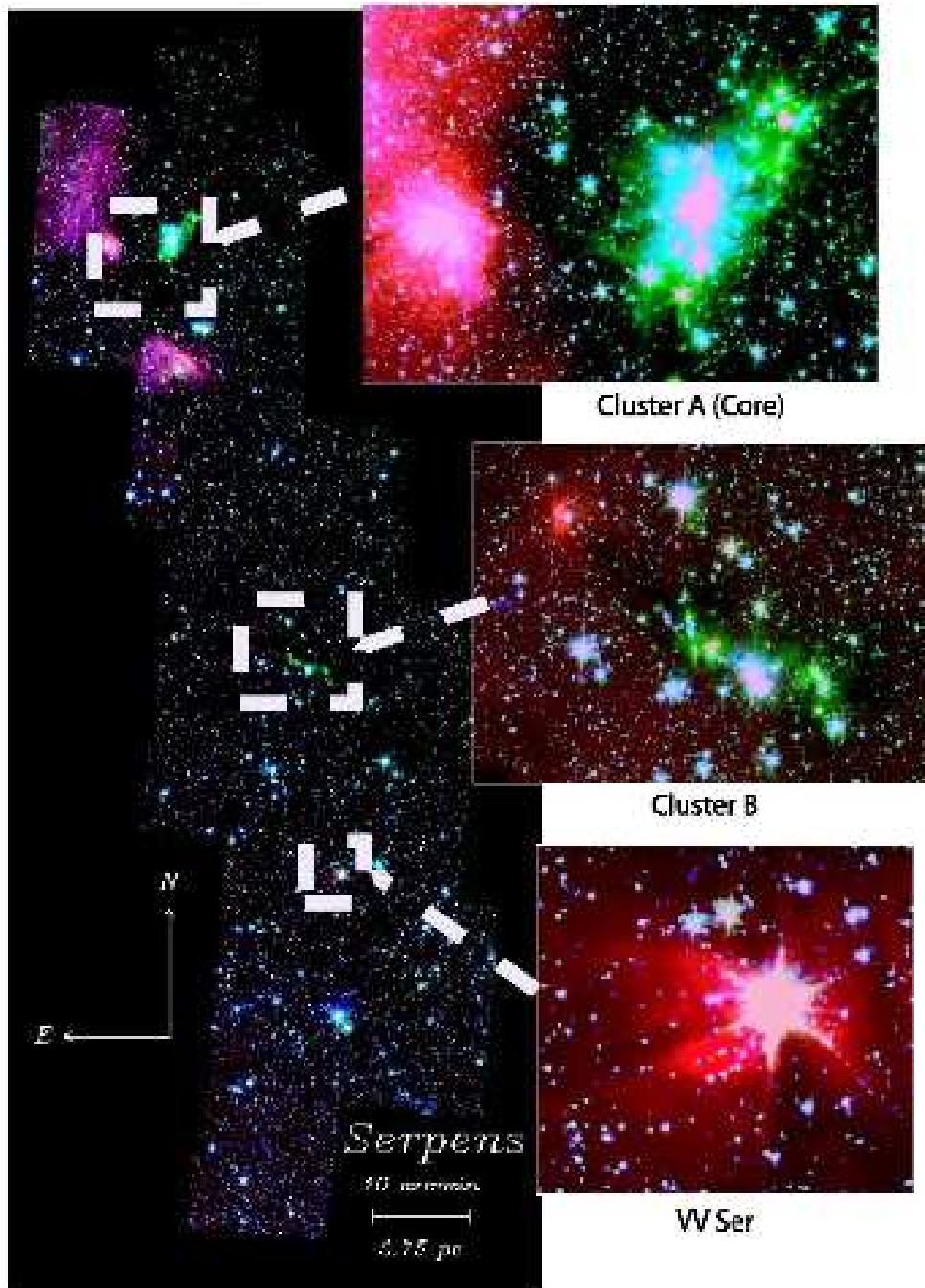


Figure 16. Colour image made from Spitzer IRAC1 (blue), IRAC2 (green), and IRAC4 (red) images. The inset images show the three Serpens stellar clusters at higher magnification. From Harvey et al. (2006).

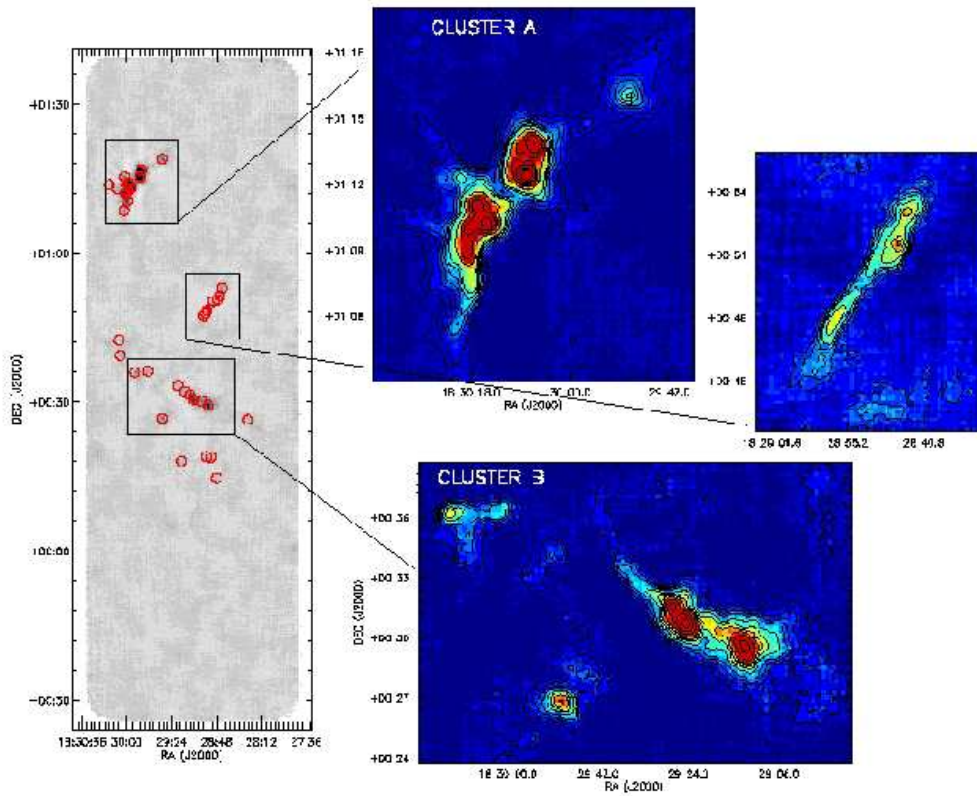


Figure 17. Bolocam 1.1 mm map of Serpens with the positions of the 35 mm sources (taken from Enoch et al. 2007).

the Serpens cloud core, has been discovered by Gutermuth et al. (2008). Radial velocities from molecular line observations of the Serpens South complex carried out by the same authors are the same as that of the Serpens core, suggesting a common distance. The cluster consists of at least 54 Class I protostars and 37 Class II sources and it has a mean surface density of 430 pc^{-2} . The median projected distance between nearest neighbor YSOs is $13''.2$ or 3700 AU - Gutermuth et al. (2008) assume a distance of 260 pc. The large fraction of Class I protostars in the Serpens South cluster, larger than in the Serpens cloud core cluster, and the high density suggest a very recent initialization of star formation and a high star formation rate, $\sim 90 M_{\odot} \text{ Myr}^{-1}$ (assuming a typical protostellar phase lifetime of 2×10^5 yr and $0.5 M_{\odot}$ per source). Doubtless, Serpens South will concentrate large observational efforts in the next future, searching for Class 0 objects, submm/mm dusty cores, outflows, etc.



Figure 18. Colour-composite of the new Serpens South cluster made from IRAC1 (blue), IRAC2 (green), and IRAC4 (red) images. From Gutermuth et al. (2008).

8. Objects of Particular Interest

The Gaseous Condensation S 68 NW: Williams & Myers (1999) detected a compact, starless core in CS (2-1) and N_2H^+ (1-0) with turbulent widths and infall asymmetry in the NW clump of the Serpens core close to S 68N, which was designated S 68NW. The line width was confirmed by Olmi & Testi (2000). This core is likely the youngest, individual evolutionary structure detected in Serpens.

SMM 4: This source is the brightest Class 0 object in the SE core clump (Casali et al. 1993, Hurt & Barsony 1996). Both Ward-Thompson & Buckley (2001) and Narayanan et al. (2002) showed that it possesses blue asymmetric line profiles in the optically thick main isotopes of HCO^+ and CS, and conclude that SMM 4 has an infalling, rotating envelope.

FIRS 1 (IRAS 18273+0113, SMM 1): FIRS 1 (Harvey et al. 1984) is the most luminous source in the Serpens core. It is a Class 0 object of $\sim 50 L_\odot$ (Casali et al. 1993, Hurt & Barsony 1996, Larsson et al. 2000). Radio continuum observations detect a triple radio jet with a non-thermal component which is interpreted as a Herbig-Haro precursor (Rodríguez et al. 1989, Curiel et al. 1993, McMullin et al. 1994). The outflowing clumps in the jet have proper motions with tangential velocities of order 200 km/s, indicating a dynamical age of only 60 years. H_2O maser and OH emission are also detected close to FIRS 1 (e.g. Moscadelli et al. 2006). Molecular outflows in different molecules are also present (White et al. 1995, Torrelles et al. 1992, Curiel et al. 1996, Williams & Myers 2000, McMullin et al. 2000). An H_2 S(1) jet emerges from the centre of FIRS 1, though it is most likely unrelated to the radio sources (Eiroa & Casali 1989, Curiel et al. 1996, Hodapp 1999).

SVS 4: Testi et al. (2000) point out that star formation in the Serpens core is very inhomogeneous, occurring in various sub-clusters. The SVS 4 complex (Eiroa & Casali 1989) is a sub-cluster of ~ 10 sources situated some $2'$ South of the SRN, containing a mix of Class I, flat-spectrum and Class II sources (Kaas et al. 2004, Pontoppidan et al. 2004, Haisch et al. 2006). Some of the objects are associated with radio continuum sources (Smith et al. 1999, Eiroa et al. 2005). It is one of the densest young stellar (sub-)clusters known, with a stellar mass density of $\sim 10^5 M_\odot \text{pc}^{-3}$ (Eiroa & Casali 1989, Pontoppidan et al. 2004). Preibisch (1998, 1999) finds EC 95 (SVS 4-9) to be one of the brightest X-ray sources known among young stars. Its high X-ray luminosity, $\sim 4 \times 10^{31} \text{erg s}^{-1}$, might be due to a very active magnetic corona, a fact partly supported by the radio spectral index (Smith et al. 1999, Forbrich et al. 2007). The infrared data places it well above the main sequence with a very young age in the range $\sim 2 - 4 \times 10^5$ years (Preibisch 1999, Pontoppidan et al. 2004). A spectrum of the CO bandhead at $2.29 \mu\text{m}$ in EC 95 indicates $v \sin(i) \sim 20\text{-}80 \text{ km s}^{-1}$ (Casali & Eiroa 1996b), and reasonably rapid rotation consistent with enhanced X-ray emission; more recently, Doppmann et al. (2005) have measured $v \sin(i) = 56 \text{ km s}^{-1}$. EC 80 (SVS 4-3), and EC 89 (SVS 4-6) are also X-ray sources (Preibisch 2004, Giardino et al. 2007).

SVS 20: SVS 20 (EC 90) is the brightest K band source in the Serpens cluster. The source contains a number of peculiar features. Observations by Eiroa et al. (1987) revealed it to be a $1.6''$ separation binary and the total luminosity and X-rays suggest

two stars of mass 1-4 M_{\odot} (Preibisch 2003). Both components have very similar near to mid-IR spectral energy distributions, although they have a brightness difference of $\Delta m \sim 1.5$ mag (Eiroa et al. 1987, Eiroa & Leinert 1987, Haisch et al. 2002) and are flat-spectrum sources (Kaas et al. 2004, Haisch et al. 2006). The K band spectrum of the brighter component, SVS 20S, is featureless, while SVS 20N has $Br\gamma$ and the 2.3 μm CO bands in emission (Fig. 8). A nebulous ring-like structure possessing spiral arm-like features, $\sim 5000 \times 3000$ AU projected onto the sky, contains shock excited H_2 emission (Eiroa et al. 1997a, see Fig 4). The correct interpretation of the nebular morphology is a matter of debate. Eiroa et al. (1997a) interpret the emission as a circumbinary disk, while studies in polarized IR radiation led Huard et al. (1997) to describe it as a cavity excavated by an outflow.

Brown Dwarfs: The near-IR object EC 64 (GCNM 57) has been identified by Lodieu et al. (2002) as a young L0-L3 brown dwarf (BD-Ser 1). It shows deep water absorption consistent with an effective temperature of 2800 K, and an estimated mass of 0.05 M_{\odot} . Klotz et al. (2004), Kaas et al. (2004), Harvey et al. (2007a) and Winston et al. (2007) have suggested further brown dwarf candidates. Furthermore, on the basis of the near-IR diagrams Eiroa et al. (2006) suggested ~ 40 near-IR Serpens objects as good brown dwarf candidates, which are now increased to more than 60 candidates, considering the Spitzer/2MASS sources. Many of them show near-IR excess denoting remarkable circumstellar disks. These objects are identified in Table 1.

Outbursts and Disappearances. EC 81 and DEOS: EC 81 was a $K = 12.2$ mag. source, with some cometary nebulosity in the original EC listing (Eiroa & Casali 1992). Yet it was invisible in the images reported in Horrobin et al. (1997) which show it to have faded by more than 3.8 magnitudes over a period of 3 years. Harvey et al. (2007a) have found several knots of emission close to the nominal position of EC 81 and have suggested that this source may have been a small clump of excited gas. By contrast, Hodapp et al. (1996) reported an FU Orionis-type outburst in a faint source (DEOS), which brightened by more than 4 magnitudes in less than 9 months. Hodapp (1988) carried out a first photometric monitoring of DEOS (Fig. 19) and showed significant changes in the spectrum of the source. More recently, Kóspál et al. (2007) has monitored this source, also called OO Serpentis, from 1996 to 2006 using ISO, Spitzer and near- and mid-IR ground-based data. Their data show that the object is fading and is likely to reach its pre-outburst brightness around 2011; those authors suggest DEOS is a Class I object with an age of $< 10^5$ yr surrounded by an accretion disk and a dense envelope.

VV Ser: VV Serpentis (Chavarría et al. 1988) has attracted considerable attention in many studies of HAe stars. In spite of this, its basic stellar parameters remain rather uncertain: spectral type between B1 and A3, luminosity class III to V, rotational velocity between 85 and 230 km s^{-1} . Ripepi et al. (2007) provide a very good summary of the current published values. Photometrically VV Ser shows deep occultations from circumstellar matter (Herbst & Shevchenko 1999, Rostopchina et al. 2001) together with δ Scuti type pulsations, suggestive of a stellar mass close to 4 M_{\odot} and an effective temperature significantly lower than the value based on the empirical spectral types (Ripepi et al. 2007). Interferometric measurements resolve the near-IR emission (Eisner et al. 2003, 2004) which is interpreted as arising from the inner parts of a disk with grains of different sizes (see also Isella et al. 2006). Double-peaked 4.7 μm CO emission is

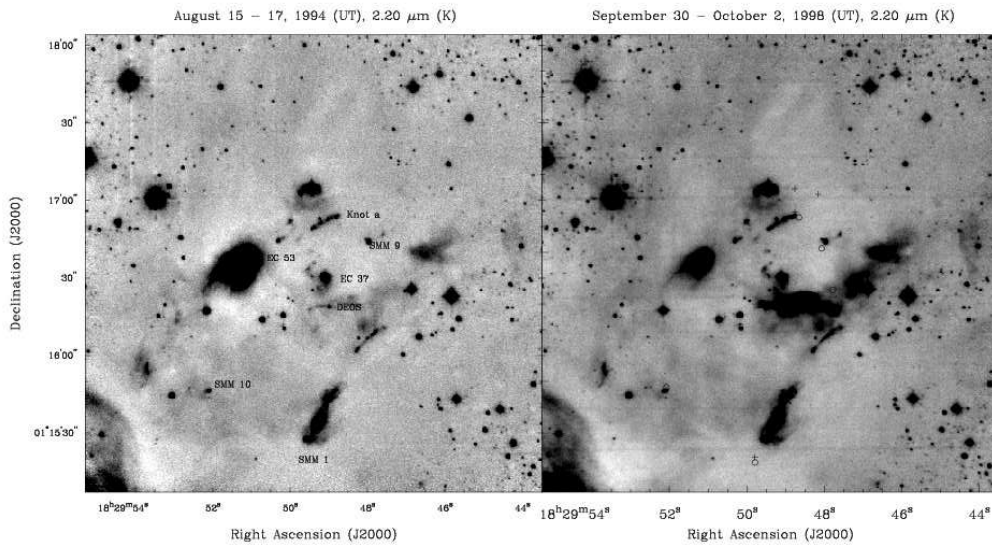


Figure 19. Combined K band images of the DEOS region in 1998 (right) and 1994 (left). DEOS and its associated luminosity to the east appear much brighter in 1998 than in 1994. Taken from Hodapp (1999).

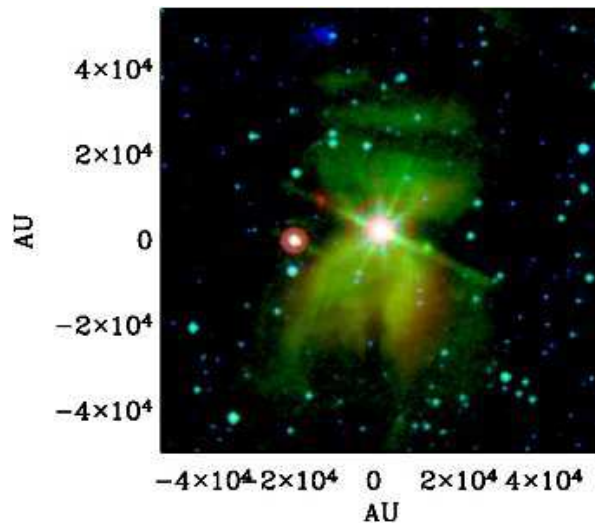


Figure 20. Spitzer composite image of VV Ser. Colours mean: $4.5 \mu\text{m}$ (blue), $8.0 \mu\text{m}$ (green), $24 \mu\text{m}$ (red). Taken from Pontoppidan et al. (2007c).

also observed (Blake & Boegert 2004). Searches for PAH emission features have been carried out by Geers et al. (2006, 2007). Spitzer IRAC and MIPS images reveal the circumstellar disk (Pontoppidan et al. 2007c) and a large, bipolar nebulosity centred on VV Ser (Fig. 20), which is interpreted as due to quantum-heated PAHs and small carbonaceous/silicates of ~ 500 atoms (Pontoppidan et al. 2007b).

Acknowledgments. It is a pleasure to thank R. A. Gutermuth, P.M. Harvey, and S.T. Megeath for providing the Spitzer results prior to publication. C.E. is supported in part by Spanish Grants AYA 2005-00954 and CAM Ref. S-0505/ESP/0361.

References

- Alexander, R. D., Casali, M. M., Andre P., Persi, P., & Eiroa, C. 2003, A&A, 401, 613
 Aspin, C. & Greene, T.P. 2007, AJ, 133, 568
 Aspin, C., Reipurth, B., & Lehmann, T. 1994, A&A, 288, 165
 Baraffe, I., Chabrier, G., Barman, T.S., Allard, F., & Hauschildt, P.H. 2003, A&A, 402, 701
 Bally, J. & Lada, C.J. 1983, ApJ, 265, 824
 Bernes, C. 1977, A&AS, 29, 65
 Blair, G.N., Davis, J.H., & Dickinson, D.F. 1978, ApJ, 226, 435
 Blake, G.A. & Boogert, A.C.A. 2004, ApJ, 606, L73
 Boogert, A.C.A., Pontoppidan, K.M., Knez, A., et al. 2008 AJ, 678, 985
 Brown, D.W., Chandler, C.J., Carlstrom, J.E., et al. 2000, MNRAS 319, 154
 Cambr esy, L. 1999, A&A, 345, 965
 Caratti o Garatti, A., Giannini, T., Nisini, B., & Lorenzetti, D. 2006, A&A, 449, 1077
 Casali, M.M. & Eiroa, C. 1996a, A&A, 306, 427
 Casali, M.M. & Eiroa, C. 1996b, in *Cool stars; stellar systems; and the Sun*, eds. R. Pallavicini & A. K. Dupree, ASP Conference Series, volume 109, p. 713
 Casali, M.M., Eiroa, C., & Duncan, W. D. 1993, A&A, 275, 195
 Chavarr a-K, C., de Lara, E., Finkenzeller, U., Mendoza, E.E., & Ocegueda, J. 1988, A&A, 197, 151
 Chiar, J. E., Adamson, A. J., Kerr, T. H., & Whittet, D. C. B. 1994, ApJ, 426, 240
 Chini, R., Reipurth, B., Sievers, A., et al. 1997, A&A, 325, 542
 Chini, R., Ward-Thompson, D., Kirk, J. M., et al. 2001, A&A, 369, 155
 Ciardi, D.R., Telesco, C. M., Packham, C., et al. 2005, ApJ, 629 897
 Clark, F.O. 1990, priv. comm.
 Clark, F.O. 1991, ApJS, 75, 611
 Clark, F.O. & Turner, B.E. 1987, A&A, 176, 114
 Cohen, M. & Kuhl, L.V. 1979, ApJS, 41, 743
 Connelley, M.S., Reipurth, B., & Tokunaga, A.T. 2007, AJ, 133, 1528
 Covey, R., Greene, T.P., Doppmann, G.W., & Lada, C.J. 2006, AJ, 131, 512
 Curiel, S., Rodr guez, L.F., G mez, J.F., et al. 1996, ApJ, 456, 677
 Curiel, S., Rodr guez, L.F., Moran, J.M., & Cant , J. 1993, ApJ, 415, 191
 Dame T.M., Hartmann, D., & Thaddeus, P. 1987, ApJ, 547, 792
 Dame T.M. & Thaddeus, P. 1985, ApJ, 297, 751
 Dame T.M., Ungerechts, H., Cohen, R.S. et al. 2001, ApJ, 322, 706
 Davis, C.J., Matthews, H.E., Ray, T.P., Dent, W.R.F., & Richer, J.S. 1999, MNRAS, 309, 141
 de Lara, E. & Chavarr a-K, C. 1989, Rev. Mex. Astron. Astrofis. 18, 180
 de Lara, E., Chavarr a-K, C., & L pez-Molina, G. 1991, A&A, 243, 139
 Dinger, A.S.C. & Dickinson, D.F. 1980, AJ, 85, 1247
 Djupvik, A.A., Andr , Ph., Bontemps, S., et al. 2006, A&A, 458, 789
 Dobashi, K., Uehara, H., Kandori, R., et al. 2005, PASJ, 57, No. SP1, S1
 Doppmann, G.W., Greene, T.P., Covet, K.R., & Lada, C.J. 2005, AJ, 130, 1145
 Dorschner, J. & G rtler, J. 1963, AN, 287, 257
 Duch ne, G., Bontemps, S., Bouvier, J., et al. 2007, A&A, 476, 229
 Eiroa, C. 1991, in *Low Mass Star Formation in Southern Molecular Clouds*, ed. Bo Reipurth, ESO Scientific Report N. 11, p. 197
 Eiroa, C. & Casali, M.M. 1989, A&A, 223, L17
 Eiroa, C. & Casali, M.M. 1992, A&A, 262, 468
 Eiroa, C., Mora, A., & Djupvik, A.A. 2008, in preparation
 Eiroa, C., Djupvik, A.A., & Casali, M.M. 2006, AN, 327, 14

- Eiroa, C. & Hodapp, K.-W 1989, A&A, 210, 345
 Eiroa, C. & Leinert, C. 1987, A&A, 188, 46
 Eiroa, C., Lenzen, R., Leinert, Ch., & Hodapp, K.-W 1987, A&A, 179, 171
 Eiroa, C.; Palacios, J., & Casali, M. M. 1997a, in *Planets Beyond the Solar System and the Next Generation of Space Missions*. ed. D. Soderblom, ASP Conference Series, Vol. 119, p.107
 Eiroa, C., Palacios, J., Eisloffel, J., Casali, M.M., & Curiel, S. 1997b, in *Herbig-Haro Flows and the Birth of Stars*, eds. B. Reipurth and C. Bertout, IAU Symposium 182, p. 103
 Eiroa, C., Torrelles, J.M., Curiel, S., & Djupvik, A.A. 2005, AJ, 130, 643
 Eiroa, C., Torrelles, J.M., Gómez, J.F., et al. 1992, PASJ, 44, 155
 Eisner, J.A., Lane, B.F., Akeson, R.L., Hildebrand, L.A., & Sargent, A.I., 2003, ApJ, 588, 360
 Eisner, J.A., Lane, B.F., Hildebrand, L.A., Akeson, R.L., & Sargent, A.I., 2004, ApJ, 613, 1049
 Enoch, M.L., Glenn, J., Evans II, N.J., et al. 2007, ApJ, 666, 982
 Evans II, N.J., Allen, L.E., Blake, G.A., et al. 2003, PASP 115, 965
 Festin, L. 1998, A&A, 336, 883
 Flaherty, K.M., Pipher, J.L., Megeath, S.T., et al. 2007, ApJ, 663, 1069
 Forbrich, J., Mass, M., Ros, E., Brunthaler, A., & Menten, K.M. 2007, A&A, 985, 992
 Fuente, A., Ceccarelli, C., Neri, R., et al. 2007, A&A, 468, L37
 Furuya, R.S., Kitamura, Y., Wootten, A., Claussen, M.J., & Kawabe, R. 2003, ApJS, 144, 71
 Geers, V.C., Augereau, J.-C., Pontoppidan, K.M., et al. 2006, A&A, 459, 545
 Geers, V.C., van Dishoeck, E.F., Visser, R., et al. 2007 A&A, 476, 279
 Giardino, G., Favata, F., Micela, G., Sciortino, S., & Winston, E. 2007, A&A, 275, 288
 Giovannetti, P., Caux, E., Nadeau, D., & Monin, J.-L. 1998, A&A, 330, 990
 Gómez de Castro, A.I 1997, A&A, 323, 541
 Gómez de Castro, A.I., Eiroa, C., & Lenzen, R. 1988, A&A, 201, 299
 Gregersen, E.M., Evans II, N.J., Zhou, S., & Choi, M. 1997, ApJ 484, 256
 Gutermuth, R.A., Bourke, T.L., Allen, L.E., et al. 2008, ApJ, 673, L151
 Gyulbudaghian, A.L., Glushkov, Yu. I., & Denisyuk, E.K. 1978, ApJ, 224, L137
 Haisch, K.E. Jr., Barsony, M., Greene, T.P., & Ressler, M.E. 2002, AJ, 124, 2841
 Haisch, K.E. Jr., Barsony, M., Ressler, M.E., & Greene, T.P. 2006, AJ, 132, 2675
 Haisch, K.E. Jr., Greene, T.P., Barsony, M., & Stahler S.W. 2004, AJ, 127, 1747
 Hartigan, P. & Lada, C. J. 1985, ApJS, 59, 383
 Harvey, P.M., Chapman, N., Lai, S.P., et al. 2006, ApJ, 644, 307
 Harvey, P.M., Merín, B., & Huard, L.T., et al. 2007a, ApJ, 663, 1149
 Harvey, P.M., Rebull, L.M., & Brooke, T., et al. 2007b, ApJ, 663, 1139
 Harvey, P.M., Wilking, B.A., & Joy, M. 1984, ApJ, 278, 156
 Herbst, T.M., Beckwith, S.V.W., & Robberto, M. 1997, ApJ, 486, L59
 Herbst, W. & Shevchenko, V.S. 1999, AJ, 118, 1034
 Ho, P.T.P. & Barrett, A.H. 1980, ApJ, 237, 38
 Hodapp, K.-W. 1999, AJ, 118, 1338
 Hodapp, K.-W., Hora, J.L., Raymer, J.T., Pickles, A.J., & Ladd, E.F. 1996, ApJ, 468, 861
 Hogerheijde, M.R., van Dishoeck, E.W., Salverda, J. M., & Blake, G. A. 1999, ApJ, 513, 350
 Horrobin, M. J., Casali, M. M., & Eiroa, C. 1997, A&A, 320, L41
 Huard, T. L., Weintraub, D. A., & Kastner, J. H. 1997, MNRAS, 290, 598
 Hurt, R.L. & Barsony, M. 1996, ApJ, 460, L45
 Hurt, R.L., Barsony, M., & Wootten, A.H. 1996, ApJ, 456, 686
 Isella, A., Testi, L., & Natta, A. 2006, A&A, 451, 951
 Kaas, A.A. 1999, AJ, 118, 558
 Kaas, A.A., Olofsson, G., Bontemps S., et al. 2004, A&A, 421, 623
 Kessler-Silacci, J., Augereau, J.-Ch., Dullemond, C.P., et al. 2006, ApJ, 639, 275
 King, D.J., Scarrott, S.M., & Taylor, K.N.R. 1983, MNRAS, 202, 1087
 Klotz, A., Caux, E., Monin, J.-L., & Lodieu, N. 2004, A&A, 425, 927
 Knez, C., Boogert, A.C., Pontoppidan, K.M., et al. 2005, ApJ, 635, L145
 Knude, J. 2005, priv. comm.
 Kóspál, Á., Ábrahám, P., Prusti, T., et al. 2007, A&A, 470, 211

- Lahuis, F., van Dishoeck, E.F., Blake, G. A., et al. 2007, ApJ, 665, 492
 Larsson, B., Liseau, R., & Men'shchikov, A.B. 2002, A&A, 386, 1955
 Larsson, B., Liseau, R., Men'shchikov, A.B., et al. 2000, A&A, 363, 253
 Little, L.J., Brown, A.T., McDonalds, G.H., Riley, P.W., & Matheson, D.N. 1980, MNRAS, 193, 115
 Lodieu, N., Caux, E., Monin, J.-L., & Klotz, A. 2002, A&A, 383, L15
 Loren, R.B., Evans, N.J., & Knapp, G.R. 1979, ApJ, 234, 932
 Loren, R.B., Plambeck, R.L., Davis, J.H., & Snell, R.L. 1981, ApJ, 245, 495
 Loren, R.B. & Wootten, A. 1980, ApJ, 242, 568
 Mardones, D., Myers, P.C., Tafalla, M., et al. 1997, ApJ, 489, 719
 McMullin, J.P., Mundy, L.G., Blake, G.A., et al. 2000, ApJ, 536, 845
 McMullin, J.P., Mundy, L.G., Wilking, B.A., Hezel, T., & Blake, G.A. 1994, ApJ, 424, 222
 Mirabel, I.F., Ruiz, A., Rodríguez L.F., & Cantó, J. 1987, ApJ, 318, 729
 Moscadelli, L., Testi, L., Furuya, R.S., et al. 2006, A&A, 446, 985
 Narayanan, G., Moriarty-Schieven, G., Walker, C.K., & Butner, H. M. 2002, ApJ, 565, 319
 Nordh, H.L., van Duinen, R.J., Sargent, A.I., et al. 1982, A&A, 115, 308
 Olmi, L. & Testi, L. 2002, A&A, 392, 1052
 Öberg, K.I., Boogert, A.C.A., Pontoppidan, K.M., et al. 2008 AJ, 678, 1032
 Palla, F. & Giovanardi, C. 1989, A&A, 223, 267
 Persi, P., Palagi, F., & Felli, M. 1994, A&A, 291, 577
 Pontoppidan, K. M., Boogert, A.C.A., Fraser, H.J., et al. 2008, AJ, 678, 1005
 Pontoppidan, K. M., Dartois, E., van Dishoeck, E. F., Thi, W.-F., & d'Hendecourt, L. 2003a, A&A, 404, L17
 Pontoppidan, K. M., Dullemond, C.P., Blake, G.A., et al. 2007b, ApJ, 656, 980
 Pontoppidan, K. M., Dullemond, C.P., Blake, G.A., et al. 2007c, ApJ, 656, 991
 Pontoppidan, K. M., Fraser, H.J., Dartois, E. et al. 2003b, A&A, 408, 981
 Pontoppidan, K. M., van Dishoeck, E. F., & Dartois, E. 2004, A&A, 426, 925
 Preibisch, T. 1998, A&A, 338, L25
 Preibisch, T. 1999, A&A, 345, 583
 Preibisch, T. 2003, A&A, 410, 951
 Preibisch, T. 2004, A&A, 428, 569
 Racine, R. 1968, AJ, 73, 233
 Reipurth, B. & Eiroa, C. 1992, A&A, 256, L1
 Reipurth, B., Nyman L.-Å, & Chini, R. 1996, A&A, 314, 258
 Reipurth, B., Rodríguez, L.F., Anglada, G., & Bally, J. 2004, AJ, 127, 1736
 Ripepi, V., Bernabei, S., Marconi, M., et al. 2007 A&A, 462, 1023
 Rodríguez, L.F., Curiel, S., Moran, J.M., et al. 1989, ApJ, 346, L85
 Rodríguez, L.F., Moran, J.M., Dickinson, D.F., & Gyulbudaghian, A.L. 1978 ApJ, 226, 115
 Rodríguez, L.F., Moran, J.M., Ho. P.T.P., & Gottlieb, E.W. 1980, ApJ, 235, 845
 Rostopchina, A.N., Grinin, V.P., & Shakhovskoi, D.N. 2001, Astron. Rep. 45, 60
 Schmeja, S., Klessen, R.S., & Froebich, D. 2005, A&A, 437, 911
 Schnee, S.L., Ridge, N.A., Goodman, A. A., & Li, J.G. 2005 ApJ, 634, 442
 Sharpless, S. 1959, ApJS, 4, 257
 Siebenmorgen, R. & Krügel, E. 2000, A&A, 364, 625
 Smith K., Guedel M., & Benz A.O. 1999, A&A, 349, 475
 Snell, R.L. & Bally, J. 1986, ApJ, 303, 683
 Sogawa, H., Tamura, M., Gatley, I., & Merrill, K.M. 1997, AJ, 113, 1057
 Straizys, V., Černis, K., & Bartasiūtė, S., 1996, Baltic Astronomy, 5, 125
 Straizys, V., Černis, K., & Bartasiūtė, S., 2003, A&A, 405, 585
 Strom, S. E., Grasdalen, G.L., & Strom, K.M. 1974, ApJ, 191, 111
 Strom, S. E., Vrba, F.J., & Strom, K.M. 1976, AJ, 81, 638
 Takano, T. 1986, ApJ, 303, 349
 Testi, L. & Sargent, A.I. 1998, ApJ, 508, L91
 Testi, L., Sargent, A.I., Olmi, L., & Onello, J.S. 2000, ApJ, 540, L53
 Torrelles, J.M., Gomez, J.F., Curiel, S., et al. 1992, ApJ, 384, 59

- Torrelles, J.M., Ho, P.T.P., Rodríguez, L.F., Canto, J., & Verdes-Montenegro, L. 1989, ApJ, 346, 756
- Ungerechts, H. & Güsten, R. 1984, A&A, 131, 177
- van den Bergh, S. 1966, AJ, 71, 990
- Ward-Thompson D. & Buckley H.D. 2000, MNRAS, 327, 95
- Warren-Smith, R.F., Draper, P.W., & Scarrott, S.M. 1987, MNRAS, 227, 749
- White, G.J., Casali, M.M., & Eiroa, C. 1995, A&A, 298, 594
- Williams, J.P. & Myers, P.C. 1999, ApJ, 518, L37
- Williams, J.P. & Myers, P.C. 2000, ApJ, 537, 891
- Winston, E., Megeath, S.T., & Wolk, S.J., et al. 2007, ApJ, 669, 493
- Wolf-Chase, G.A., Barsony, M., Wootten H.A., et al. 1998, ApJ, 501, L193
- Worden, S.P. & Grasdalen, G.L. 1974, A&A, 34, 37
- Wu, J., Dunham, M.M., Evans, N.J., II, Bourke, T.L., & Young, C.H. 2007, AJ, 133, 1560
- Wu, J.W., Wu, Y.F., Wang, J.Z., & Cai, K. 2002, Chin. J. Astron. Astrophys. 2, 33
- Zhang, C.Y. Laureijs, R.J., & Clark, F.O. 1988a, A&A, 196, 236
- Zhang, C.Y. Laureijs, R.J., Clark, F.O., & Wesselius, P.R. 1988b, A&A, 199, 170
- Ziener, R. & Eislöffel, J. 1999, A&A, 347, 565

Table 1. Near-IR sources embedded in the Serpens clouds.

No.	α_{2000}	δ_{2000}	J	H	K		Name
1	18 29 04.3	01 18 39	16.7	16.0	15.5	!	WMW72
2	18 29 05.8	01 13 23	16.3	15.8			WMW97
3	18 29 08.2	01 05 45	10.7	10.2	10.1		WMW124
4	18 29 13.0	01 07 01	8.8	7.3	6.6		WMW122
5	18 29 14.3	01 07 30	14.6	13.7	13.2	!	WMW53
6	18 29 16.4	01 08 22	16.3	15.3	14.8	!	WMW136
7	18 29 20.4	01 21 04	12.8	11.3	10.3		WMW104
8	18 29 21.1	01 24 07	16.3	15.4	14.8	!	WMW57
9	18 29 22.7	01 10 33	12.2	11.1	10.9		WMW221
10	18 29 31.6	01 15 06	16.0	14.7	14.2	!	WMW224
11	18 29 31.9	01 18 42	11.6	9.8	8.4		ESO H α 279a/WMW36
12	18 29 31.8	01 18 34	17.0	12.5	9.9		ESO H α 279b#
13	18 29 32.2	01 12 40	16.3	15.7	14.9	!	WMW75
14	18 29 33.1	01 17 17	11.4	10.3	10.0		WMW225
15	18 29 33.4	01 08 24	9.8	9.4	9.2		WMW82
16	18 29 34.1	01 17 29	14.8	12.5	11.4		KCML14
17	18 29 35.2	01 13 11	15.5	14.5	13.7	!	WMW91
18	18 29 37.5	01 14 54	14.5	13.1	12.4		KCML13
19	18 29 37.6	01 11 18	11.2	9.3	8.5		WMW134
20	18 29 37.7	01 11 30	11.5	9.6	8.8		WMW127
21	18 29 38.2	01 09 18	15.9	14.8	14.5	!	WMW64
22	18 29 39.8	01 17 12	15.3	12.9	11.8		KCML12
23	18 29 39.9	01 17 56	14.5	12.8	11.9		WMW94
24	18 29 41.4	01 07 39	11.6	10.6	9.7		STGM3/WMW103
25	18 29 41.5	01 10 05	12.9	11.1	10.3		WMW176
26	18 29 41.9	01 17 13	18.6	15.4	13.7		KCML11
27	18 29 42.2	01 20 21	13.3	12.5	12.0		WMW93
28	18 29 42.4	01 12 02	16.7	14.1	12.8		KCML6/WMW215
29	18 29 42.5	01 16 19	21.1	17.1	15.0		KCML10
30	18 29 43.1	01 15 00	17.0	15.2	14.2		EC1/KCML9
31	18 29 43.8	01 07 21	13.7	12.5	11.6		STGM2/WMW65
32	18 29 43.8	01 10 47	13.6	11.8	11.0		KCML5
33	18 29 44.3	01 04 54	8.5	6.6	5.4		WMW71
34	18 29 44.4	01 13 11	13.3	12.1	11.7	*	EC11/WMW100
35	18 29 44.7	01 13 51	17.0	14.0	12.4		EC12/KCML8
36	18 29 44.7	01 15 39		15.1	13.5	*	EC13
37	18 29 44.9	01 19 57	14.7	13.6	12.9		STGM34
38	18 29 45.7	01 11 12	16.2	14.4	13.4		KCML4
39	18 29 46.0	01 16 23		13.7	11.8		EC21
40	18 29 46.1	01 13 47		13.9	12.1		EC22
41	18 29 46.1	01 15 39			17.3		K1
42	18 29 46.2	01 08 56	16.2	15.3	14.8	!	BD-Ser2
43	18 29 46.3	01 10 25	13.2	12.3	11.9		WMW79
44	18 29 46.3	01 12 12	13.3	11.7	11.1		EC23
45	18 29 46.4	01 12 21		14.7	14.3	!	EC25/K2
46	18 29 46.6	01 12 07			14.1		K3
47	18 29 46.5	01 14 33	18.4	17.7	16.9	!	K4
48	18 29 46.8	01 16 08			14.3	*	EC26
49	18 29 47.0	01 16 26			13.4	*	EC28/WMW5
50	18 29 47.2	01 07 16	15.9	14.8	14.4	!	WMW68
51	18 29 47.2	01 13 14			16.1		K5

Table 1. Continuation.

No.	α_{2000}	δ_{2000}	J	H	K	Name
52	18 29 47.2	01 22 35	11.8	10.5	10.10	WMW199
53	18 29 47.3	01 16 01	18.6	17.6	15.8	! K6/BD-Ser3
54	18 29 47.4	01 14 03		18.1	14.5	EC29,GCNM1
55	18 29 47.8	01 12 16	17.1	15.7	15.1	+,! EC30,GCNM2
56	18 29 47.9	01 11 18	16.5	15.4	14.1	STGM5
57	18 29 48.1	01 16 45			16.5	SMM9-IR/WMW23
58	18 29 48.2	01 13 04	18.9	18.4	17.7	! K7
59	18 29 48.5	01 13 04	16.2	14.8	14.2	+,! EC32,GCNM8
60	18 29 48.7	01 13 42	17.6	14.9	13.5	EC33/GCNM13/K8/ KCML7/WMW106
61	18 29 49.0	01 12 51			16.6	K9
62	18 29 49.0	01 13 00	15.5	13.7	12.8	EC36/GCNM18
63	18 29 49.1	01 16 21			10.8	DEOS/K4_5/WMW11
64	18 29 49.2	01 16 32			13.2	EC37/GCNM19/ WMW6
65	18 29 49.5	01 12 04	16.2	14.8	14.4	! WMW218
66	18 29 49.5	01 17 07		15.8	12.5	EC38/WMW7
67	18 29 49.6	01 14 57			14.7	* EC40/GCNM22/ WMW48
68	18 29 49.6	01 15 29			14.6	EC41/GCNM23/ WMW114
69	18 29 49.7	01 13 49		16.1	14.1	+ EC42/GCNM25
70	18 29 49.8	01 12 33	17.3	16.0	14.8	! EC43/GCNM26
71	18 29 50.2	01 12 17	17.5	16.5	14.7	EC45/GCNM29
72	18 29 50.3	01 12 41	18.4	17.3	16.0	! K10
73	18 29 50.6	01 12 14	18.5	17.2	16.1	! K11
74	18 29 50.5	01 08 58	14.4	13.0	12.5	WMW209
75	18 29 50.5	01 13 26			17.3	K12
76	18 29 50.5	01 12 23	18.2	17.1	15.2	EC47/GCNM32
77	18 29 50.8	01 16 15			14.9	+ EC49/GCNM33
78	18 29 51.2	01 13 20	15.8	14.3	13.4	EC51/GCNM35/ WMW95
79	18 29 51.2	01 12 41		17.4	15.2	EC50/GCNM36
80	18 29 51.2	01 16 40	15.9	12.7	10.9	EC53/STGM27/ WMW24
81	18 29 51.4	01 09 33	15.7	15.0		WMW66
82	18 29 51.6	01 13 14		16.5	15.5	! GCNM40/K13
83	18 29 51.9	01 14 42			16.5	K14
84	18 29 51.9	01 14 45			15.6	K15
85	18 29 52.0	01 13 22	17.1	14.7	13.3	EC56/GCNM44/K16
86	18 29 52.2	01 15 48			15.9	SMM10-IR/WMW21
87	18 29 52.2	01 16 18	17.9	15.3	13.8	EC58/GCNM45/K17
88	18 29 52.1	01 13 23	19.4	16.0	14.5	EC57/GCNM46/K18
89	18 29 52.4	01 12 47	19.0	14.5	12.5	EC59/GCNM47
90	18 29 52.5	01 14 23			14.5	GCNM48/K19
91	18 29 52.6	01 14 45			15.3	K20
92	18 29 52.7	01 13 10		15.6	14.1	EC61/GCNM50/K21
93	18 29 52.6	01 13 26			15.5	EC60/GCNM51
94	18 29 52.5	01 19 33	16.8	15.4	14.3	! STGM33
95	18 29 52.8	01 14 36	17.5	16.1	15.2	! GCNM52/K22
96	18 29 52.8	01 14 55			14.1	GCNM53

Table 1. Continuation.

No.	α_{2000}	δ_{2000}	J	H	K	Name
97	18 29 53.1	01 06 18	14.4	13.1	12.6	WMW96
98	18 29 53.1	01 15 46			14.8	* EC63/GCNM55
99	18 29 53.1	01 14 28		16.9	15.9	! GCNM56/K23
100	18 29 53.1	01 12 28	17.3	15.4	14.4	! EC64/GCNM57/ BD-Ser1/WMW86
101	18 29 53.2	01 14 38			15.9	K24
102	18 29 53.4	01 14 23	16.9	14.9	13.2	+ EC65/GCNM59
103	18 29 53.4	01 17 01	12.7	11.3	10.6	EC67/GCNM60/STGM29/ WMW81
104	18 29 53.4	01 13 06	14.9	14.1	13.5	! EC66/GCNM61/STGM14/ WMW99
105	18 29 53.8	01 12 47			15.1	WMW34
106	18 29 53.8	01 13 31	16.5	14.2	12.9	EC68/GCNM63/WMW69
107	18 29 54.0	01 07 11	15.3	14.2	13.1	STGM1/WMW39
108	18 29 54.0	01 12 19			16.4	K25
109	18 29 54.0	01 14 07	19.7	18.1	16.7	! K26
110	18 29 54.0	01 14 36	18.7	16.4	15.8	! GCNM66/HCE165/K27
111	18 29 54.1	01 14 43		15.5	15.3	GCNM68/HCE166/K29
112	18 29 54.0	01 20 19	15.8	14.5	13.6	STGM36
113	18 29 54.3	01 12 19			16.2	K28
114	18 29 54.2	01 16 36			17.9	K30
115	18 29 54.3	01 15 03	15.7	12.6	10.9	EC69/GCNM69/CK10/ STGM23
116	18 29 54.3	01 18 17	15.3	14.8	14.3	! STGM31
117	18 29 54.5	01 14 48	14.4	13.3	12.8	EC70/GCNM70/WMW87
118	18 29 54.5	01 16 54			14.2	+ EC71/GCNM71
119	18 29 55.1	01 11 23	16.5	15.0	14.0	! STGM6
120	18 29 55.2	01 13 23	15.6	13.2	12.1	EC73/GCNM75/STGM15/ K2_1/WMW62
121	18 29 55.6	01 08 34		14.8	14.3	! WMW56
122	18 29 55.3	01 10 34	14.0	13.4	12.9	WMW201
123	18 29 55.6	01 14 30	15.0	12.3	10.7	EC74/GCNM76/CK9/ STGM21/K2_3/WMW38
124	18 29 55.9	01 11 29	18.8	18.6	18.0	! K31
125	18 29 55.8	01 15 07	18.3	17.0	14.2	EC75/GCNM77
126	18 29 55.9	01 15 11		17.1	14.5	EC76/GCNM78
127	18 29 56.2	01 10 58	12.5	11.7	11.4	WMW205
128	18 29 56.3	01 12 18	15.3	14.2	13.6	! EC77/GCNM80/STGM9/ WMW204
129	18 29 56.1	01 20 04	16.6	15.3	14.3	! STGM35
130	18 29 56.4	01 13 20			17.3	K32/WMW112
131	18 29 56.4	01 15 32		17.9	15.0	+ GCNM83/HCE169
132	18 29 56.5	01 13 01	14.8	12.5	11.4	EC79/GCNM84/STGM12/ WMW80
133	18 29 56.5	01 12 41			13.6	EC80/GCNM85/WMW61
134	18 29 56.8	01 13 31		12.8	12.2	EC81
135	18 29 56.8	01 14 46	11.9	10.3	8.8	SVS2/EC82/GCNM87/ CK3/STGM22/WMW9
136	18 29 56.7	01 15 50		17.3	15.6	+,! GCNM88/HCE172
137	18 29 56.8	01 16 09	16.1	15.7	14.9	! EC83/GCNM89

Table 1. Continuation.

No.	α_{2000}	δ_{2000}	J	H	K	Name
138	18 29 56.8	01 12 49	15.0	12.4	11.0	EC84/GCNM90/STGM11/ WMW85
139	18 29 57.1	01 11 29	16.5	15.2	14.0	STGM7
140	18 29 57.0	01 15 41		17.1	15.7	! HCE173
141	18 29 57.1	01 16 35	16.0	14.4	13.6	! EC85/GCNM91
142	18 29 57.2	01 12 59			15.3	GCNM92/HCE174
143	18 29 57.3	01 14 50	13.3	11.5	10.8	EC86/GCNM93/WMW190
144	18 29 57.4	01 13 50	18.3	15.5	13.4	EC87/GCNM94/K2_4
145	18 29 57.5	01 13 02			11.7	EC88/GCNM96/CK5
146	18 29 57.5	01 13 06	15.9	13.5	11.6	EC89/GCNM97/STGM13
147	18 29 57.6	01 14 05	12.2	9.3	6.7	SVS20S/EC90/GCNM98/ CK1/STGM18
148	18 29 57.6	01 14 07				SVS20N
149	18 29 57.6	01 10 47	9.2	9.1	9.1	WMW193
150	18 29 57.7	01 10 54	8.1	8.1	8.1	WMW192
151	18 29 57.7	01 15 31	15.8	12.8	10.8	EC93/GCNM100/STGM25/ CK12/WMW83
152	18 29 57.7	01 12 28		15.4	12.6	EC91/GCNM101/WMW70
153	18 29 57.8	01 12 39		14.1	11.4	EC94/GCNM102/WMW37
154	18 29 57.8	01 12 47	16.7	12.3	9.8	EC95/GCNM103
155	18 29 57.7	01 12 52	15.4	12.0	10.2	EC92/GCNM104
156	18 29 58.2	01 15 21	13.0	11.0	9.8	EC97/GCNM106/CK4/ STGM24/WMW27
157	18 29 58.1	01 15 57			16.1	GCNM107/K33
158	18 29 58.3	01 16 22			15.3	K34
159	18 29 58.4	01 12 51		14.6	12.3	EC98/GCNM110
160	18 29 58.5	01 16 20			11.0	GCNM111
161	18 29 58.8	01 14 25	16.7	14.2	12.3	EC103/GCNM112/STGM20/ K2_5/WMW4
162	18 29 58.7	01 16 21	13.0	11.4	10.7	EC100/GCNM113
163	18 29 58.7	01 13 17			13.4	EC101
164	18 29 58.7	01 13 04			15.4	EC102/GCNM114
165	18 29 58.8	01 15 03			14.8	EC104
166	18 29 59.0	01 12 25			14.6	* GCNM115/HCE175/WMW45
167	18 29 59.1	01 14 41			14.3	EC106/GCNM116/K35
168	18 29 59.1	01 11 20	14.2	12.6	11.9	WMW196
169	18 29 59.1	01 11 14			14.4	WMW198
170	18 29 59.3	01 08 11	16.3	14.5	13.2	STGM4
171	18 29 59.2	01 16 27			15.9	+ EC107/GCNM118
172	18 29 59.1	01 14 09	12.6	10.5	9.8	EC105/GCNM119/CK8/ STGM19/K2_6
173	18 29 59.2	01 12 28			15.3	GCNM120
174	18 29 59.6	01 11 57			14.1	K2_7/HB1/WMW3
175	18 29 59.5	01 15 54		17.2	14.9	+ GCNM123/HCE176
176	18 29 59.5	01 14 53		17.2	15.3	EC109/GCNM124
177	18 30 00.0	01 14 04	15.6	14.0	12.8	EC114/GCNM131/STGM17/ WMW28
178	18 30 00.1	01 03 06	14.2	12.7	12.1	WMW156
179	18 30 00.2	01 14 45		16.3	15.0	! EC116/GCNM132/K36
180	18 30 00.5	01 13 40	13.3	11.1	10.1	EC117/GCNM135/CK6/ WMW216

Table 1. Continuation.

No.	α_{2000}	δ_{2000}	J	H	K	Name
181	18 30 00.5	01 15 19	18.0	12.6	8.9	EC118/GCNM136/CK2/ WMW158
182	18 30 00.9	01 16 51	16.4	15.1	14.2	! EC120/GCNM141
183	18 30 00.9	01 22 04	15.9	15.1	14.5	! WMW77
184	18 30 01.0	01 13 24		15.3	12.8	EC121/GCNM142/WMW30
185	18 30 01.1	01 15 05	15.5	13.2	12.0	EC122/GCNM146/CK12/ WMW195
186	18 30 01.5	01 15 15	15.7	15.0	15.1	EC123/GCNM148/K37/ SVS1/WMW31
187	18 30 01.5	01 20 36	15.8	14.9	14.2	! STGM37
188	18 30 01.7	01 04 43	16.1	14.2	13.1	WMW92
189	18 30 01.9	01 14 01	16.0	14.6	12.6	EC125/GCNM154/CK7/ STGM16/WMW1
190	18 30 02.4	01 12 45			15.5	+ EC128/GCNM156/WMW47
191	18 30 02.4	01 14 15			17.0	+ EC127/GCNM157
192	18 30 02.7	01 12 30	15.2	11.8	10.0	EC129/GCNM160/STGM10/ WMW10
193	18 30 02.8	01 16 16			15.4	+ EC132/GCNM162
194	18 30 02.8	01 13 23	15.7	15.3	14.7	! EC131/GCNM163
195	18 30 03.0	01 18 11	14.0	13.2	12.6	STGM30
196	18 30 03.0	01 19 50	16.3	15.9	15.1	! WMW189
197	18 30 03.3	01 16 20	12.6	10.8	10.3	EC135/GCNM165/STGM26/ WMW78
198	18 30 03.5	01 16 15	14.3	13.4	13.0	! EC138
199	18 30 03.6	01 16 41			14.2	WMW174
200	18 30 03.6	01 15 04			16.4	K38
201	18 30 03.6	01 12 41	16.2	13.4	12.2	* EC141
202	18 30 03.7	01 16 10		15.7	13.6	EC142
203	18 30 04.1	01 06 56	16.8	14.9	14.2	! WMW60
204	18 30 04.9	01 12 12			16.1	K39
205	18 30 04.8	01 14 41	13.7	12.8	12.3	EC149/WMW98
206	18 30 04.9	01 12 37	16.0	14.3	13.6	! EC152/K40/WMW54
207	18 30 05.5	01 14 25	15.2	14.4	14.1	! WMW203
208	18 30 05.7	01 13 50	17.0	13.9	12.2	EC160
209	18 30 05.9	01 13 46		14.0	12.5	EC161
210	18 30 05.9	01 21 42	14.8	14.0	13.3	STGM38
211	18 30 06.1	01 06 17	12.9	11.8	11.2	WMW84
212	18 30 06.9	01 18 24	14.8	13.7	12.9	STGM32
213	18 30 07.7	01 12 05	12.2	10.9	10.0	STGM8/WMW73
214	18 30 08.3	01 11 39	19.2	17.9	16.9	! K42
215	18 30 08.2	01 12 41			14.4	K41
216	18 30 08.6	01 17 01	17.1	14.9	13.2	STGM28
217	18 30 08.8	01 12 02	16.1	14.6	13.7	! K43
218	18 30 08.9	01 15 47			14.3	K44
219	18 30 09.2	01 17 53	15.4	14.0	13.0	WMW67
220	18 30 09.3	01 14 07	18.4	16.6	15.2	! K45
221	18 30 09.4	01 02 47	10.6	8.9	8.1	WMW170
222	18 30 09.7	01 15 21	18.6	17.9	16.8	! K46
223	18 30 10.6	01 16 21	19.2	18.5	17.1	! K47
224	18 30 11.2	01 12 12	16.8	15.2	14.2	! K48
225	18 30 11.1	01 12 57	17.5	16.3	15.2	! K49

Table 1. Continuation.

No.	α_{2000}	δ_{2000}	J	H	K	Name
226	18 30 11.1	01 12 38		12.5	12.0	WMW101
227	18 30 11.6	01 13 57			14.4	K50
228	18 30 12.0	01 16 45			8.7	K51/SVS6
229	18 30 12.3	01 17 45			15.7	K52
230	18 30 12.5	01 15 33			15.1	K53
231	18 30 13.3	01 02 49	13.7	12.8	12.4	WMW74
232	18 30 13.3	01 15 31			15.8	K54
233	18 30 13.5	01 12 18			16.4	K55
234	18 30 13.3	01 17 46			16.8	K3_11
235	18 30 14.0	01 08 52	13.8	12.7	12.4	WMW166
236	18 30 14.4	01 04 06	15.3	14.3	13.9	! WMW89
237	18 30 15.4	01 17 30			15.8	K56
238	18 30 15.6	01 17 31			14.6	K57
239	18 30 16.8	01 19 17	16.2	15.8	15.2	! WMW187
240	18 30 17.0	01 13 08	16.5	15.2	14.2	! WMW76
241	18 30 17.3	01 21 33	9.7	8.2	7.5	WMW161
242	18 30 18.2	01 14 17	13.3	11.8	10.9	WMW40
243	18 30 22.4	01 20 44	13.1	12.2	11.9	WMW157
244	18 30 22.7	01 13 24	16.0	15.0	14.6	! WMW58
245	18 30 22.8	01 16 21	15.6	14.4	13.6	! WMW55
246	18 30 23.1	01 20 10	13.3	12.6	12.2	WMW128
247	18 30 23.4	01 05 05	13.4	12.4	11.8	WMW33
248	18 30 24.4	01 19 51	12.4	11.9	11.8	WMW220
249	18 30 27.7	01 22 35	15.9	15.3	14.5	! WMW102
250	18 30 37.3	01 16 09	10.4	8.8	8.2	WMW140
251	18 30 41.2	01 13 16	14.5	13.7	13.2	! WMW88
252	18 30 44.5	01 23 30		14.7	14.5	! WMW90
253	18 30 53.7	01 11 21	11.1	9.6	8.9	WMW143

(\\$) Labels correspond to the following references: ESO Ha 279a: Aspin et al. 1994; EC: Eiroa & Casali 1992; GCNM: Giovannetti et al. 1998; STGM: Sogawa et al. 1997; K: Kaas 1999; SMM9, SMM10: Hodapp 1999; DEOS: Hodapp et al 1996; BD-Ser, KCML: Klotz et al. 2004; HCE: Horrobin et al. 1997; CK: Churchwell & Koorneef 1986; SVS: Strom et al. 1976, HB: Hurt & Barsony, 1996; WMW: Winston et al. (2007) (#) Recent spectra show that this object is in fact a background M-type giant star (Aspin & Greene, 2007). (*) Identified using ISO data (Kaas et al. 2004). (+) Serpens object candidate suggested in this work based on K -brightness variability ($\Delta K > 0.5$ mag. (!) Brown dwarf candidates suggested in this work.

Table 2. Cross-correlation of the near-IR source names with other wavelength names.

No.	Optical	Near-IR	ISO	Spitzer	Submm	VLA	XMM	Chandra	Class
11		ESO H α 279a/WMW36	159	104			9		flat
12		ESO H α 279b	160						II
24		STGM3/WMW103	207						II
28		KCML6/WMW215						21	III
31		STGM2/WMW65	219	125					II
34		EC11/WMW100	224	128				23	II
36		EC13	226						II
39		EC21	231						II
44		EC23	232						II
48		EC26	234						flat
49		EC28/WMW5	237	131					I,flat
57		SMM9-IR/WMW23	241	135	SMM9	VLA5			0,I
60		EC33/GCNM13/K8/ KCML7/WMW106	242						II
63		DEOS/K4.5/WMW11	250	137					I
64		EC37/GCNM19/ WMW6	249	138					I
66		EC38/WMW7	254	139				28	I
67		EC40/GCNM22/ WMW48	253	142					I
68		EC41/GCNM23/ WMW114	258a		SMM1	VLA7			0,I
78		EC51/GCNM35/ WMW95	266	147				31	II
80		EC53/STGM27/ WMW24	265		SMM5	VLA9	182951.2+011640	30	I
85		EC56/GCNM44/K16	266						II
86		SMM10-IR/WMW21	270	150	SMM10	VLA10			0,I
89		EC59/GCNM47	272						II
96		GCNM53	276			VLA11		33	I

Table 2. Continuation.

No.	Optical	Near-IR	ISO	Spitzer	Submm	VLA	XMM	Chandra	Class
98		EC63/GCNM55	277						I
100		EC64/GCNM57/ BD-Ser1/WMW86		160					II
103		EC67/GCNM60/ STGM29/WMW81	283	162			182953.7+011702	34	II
104		EC66/GCNM61/ STGM14/WMW99	279						II
106		EC68/GCNM63/ WMW69	285	163					II
107		STGM1/WMW39		164					flat
115		EC69/GCNM69/ CK10/STGM23	289						II
117	GEL2	EC70/GCNM70/ WMW87	291					35	II
120	GEL3	EC73/GCNM75/K2_1/ STGM15/WMW62	294	168					flat
123	GEL4	EC74/GCNM76/CK9/ STGM21/K2_3/WMW38	298	171			182955.7+011428	37	II
128		EC77/GCNM80/ STGM9/WMW204						39	III
132	GEL5	EC79/GCNM84/ STGM12/WMW80	304	174		VLA12		40	II
133		EC80/GCNM85/ WMW61	306	175				42	I
135	GEL6	SVS2/EC82/CK3/ GCNM87/STGM22/WMW9	307	176				43	flat
138	GEL7	EC84/GCNM90/ STGM11/WMW85	309			VLA14		44	II

Table 2. Continuation.

No.	Optical	Near-IR	ISO	Spitzer	Submm	VLA	XMM	Chandra	Class
143	GEL8	EC86/GCNM93/ WMW190					182757.5+011448	45	III
144		EC87/GCNM94/ /K2_4	313						I
145	GEL9	EC88/GCNM96/ CK5	312	179		VLA15		46	I
146		EC89/GCNM97/ STGM13	312	181					
147	GEL10	SVS20S/EC90/CK1 GCNM98/STGM18/WMW35	314	182	SMM6	VLA16	182957.7+011407	48	flat
148		SVS20N	314						flat
151		EC93/GCNM100/ STGM25/CK12/WMW83	319	183			182957.9+011530	50	II
152		EC91/GCNM101/ WMW70	320	184					flat
153		EC94/GCNM102/ WMW37	318	186				52	flat
154		EC95/GCNM103	317	187		VLA17	182957.9+011246	53	II
155		EC92/GCNM104	317	185		VLA17'			I
156	GEL12	EC97/GCNM106/ CK4/STGM24/WMW27	321	188			182958.4+011520	55	II
159		EC98/GCNM110	322					56	flat
161		EC103/GCNM112/ STGM20/K2_5/WMW4	326	190					I
166		GCNM115/HCE175/ WMW46	327	192					I
172	GEL13	EC105/GCNM119/ CK8/STGM19/K2_6/WMW59	328	194			182959.3+011408	59	II
174		K2_7/HB1/WMW3	330	197			+	60	I

Table 2. Continuation.

No.	Optical	Near-IR	ISO	Spitzer	Submm	VLA	XMM	Chandra	Class
177	GEL14	EC114/GCNM131/ STGM17/WMW28		200				62	I/II
180	GEL15	EC117/GCNM135/ CK6/WMW216	338			VLA20	183000.7+011338	65	II
184		EC121/GCNM142/ WMW30	341	204				66	flat
185	GEL16	EC122/GCNM146/ CK12/WMW195					183001.3+011500	67	III
189		EC125/GCNM154/ CK7/STGM16/WMW1	345	207					flat
192		EC129/GCNM160/ STGM10/WMW10	347	208					flat
197	GEL18 GGD29	EC135/GCNM165/ STGM26/WMW78	348	209			183003.5+011620	69	II
201		EC141	351						II
205		EC149/WMW98		215				71	II
206		EC152/K40/WMW54	356	216					II
213		STGM8/WMW73	366	220			183007.7+011204	75	II

(!) Labels in the different columns correspond to the following references: column 1: numbers of the near-IR objects in Table 1; column 2: Gómez de Castro et al. (1988); column 3: references as in Table 1; column 4: Kaas et al. (2004); column 5: Harvey et al. (2007a); column 6: Casali et al. (1993), Davis et al. (1999); column 7: Eiroa et al. (2005); column 8: Preibisch (2003,2004); column 9: Giardino et al. (2007); column 10: evolutionary classes taken from Kaas et al. (2004), Eiroa et al. (2005), and Winston et al. (2007).